Accelerated Design of Cost-Effective Thermal/Environmental Barrier Coatings based on High-Entropy Rare Earth Disilicates: A First-Principles Study

Shiqiang Hao[1,2], Richard Oleksak[1], Omer Dogan[1] and Michael Gao[1]

[1]National Energy Technology Laboratory, Albany, OR 97321, USA
[2]NETL Support Contractor, Albany, OR 97321, USA

August 22, 2024

NATIONAL ENERGY TECHNOLOGY LABORATORY

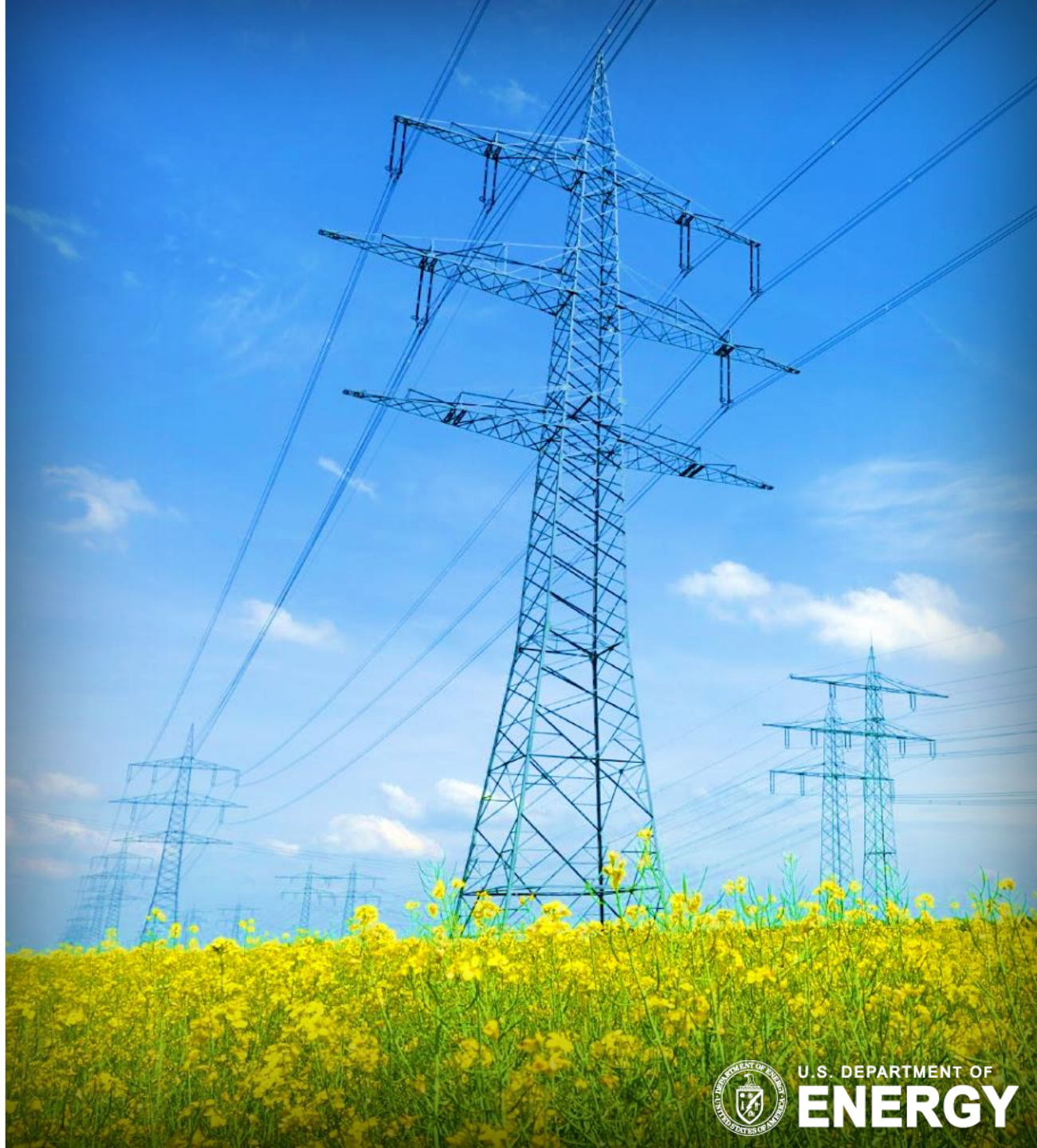

Introduction

- **Gas turbine engines** have a huge impact on the transportation, energy, and defense sectors of the global economy.
- Experience **extremely high temperatures** (e.g., up to 1800 K) with **corrosive species** in the exhaust gas.
- **SiC-based ceramic matrix composites** can fulfil the stringent requirements to provide an increased service temperature and superior strength at high temperatures.
- Under these harsh conditions, thermal/environmental barrier coatings (**TEBCs**) are required.

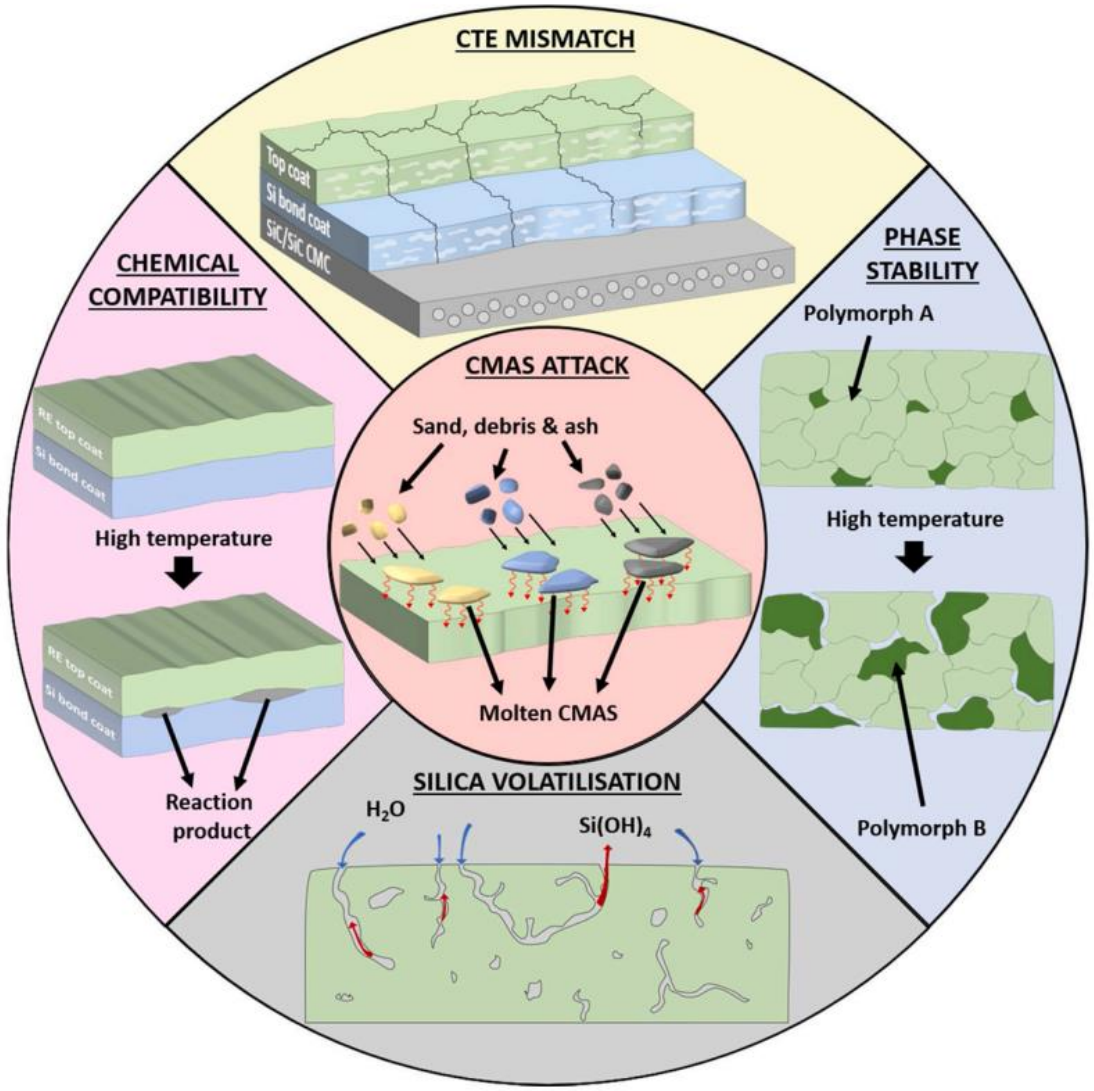

D. Tejero-Martin, C. Bennett, T. Hussain J. Eur Cer. Soc. 41, (2021) 1747-1768

Introduction & Approaches

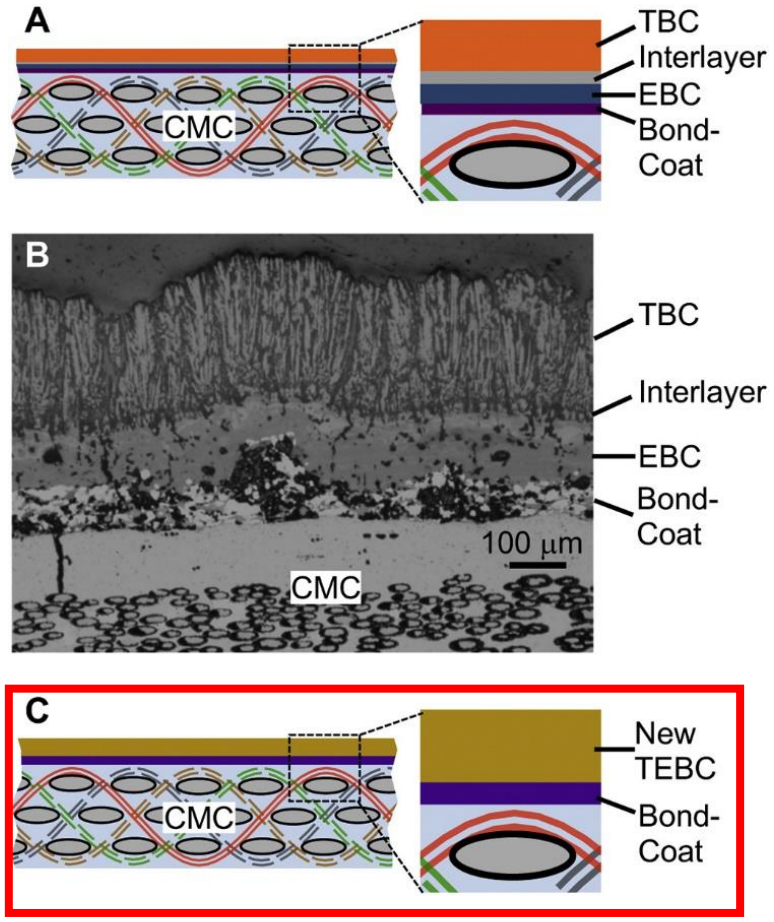

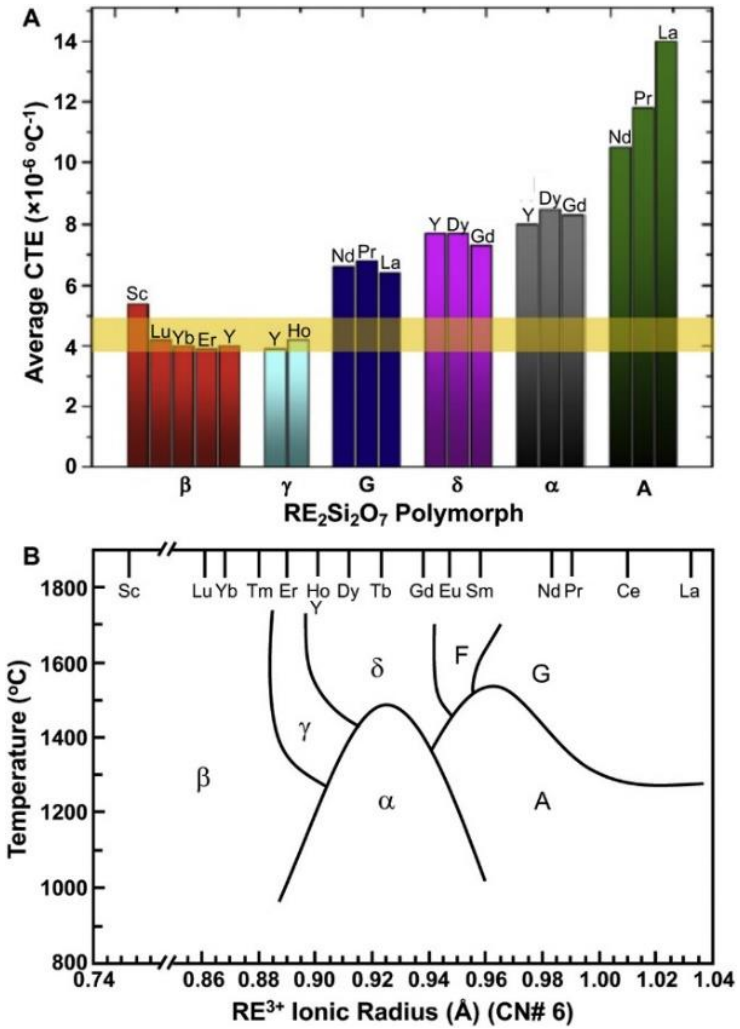

- Corrosion resistance against CMAS attack
- Corrosion resistance against water vapor
- Low thermal conductivity (ideally < 1 $Wm^{-1}K^{-1}$)
- CTE match with CMC
- Phase stability at high temperatures
- Fracture toughness

First principles density functional theory calculations to predict:

- ❖ Structure
- ❖ Lattice thermal conductivity
- ❖ Coefficient of thermal expansion
- ❖ Temperature-dependent elastic properties

L.R. Turcer, N.P. Padture, Scripta Mater. 154 (2018) 111-117

Atomic Structure of $Y_2Si_2O_7$ and $Yb_2Si_2O_7$

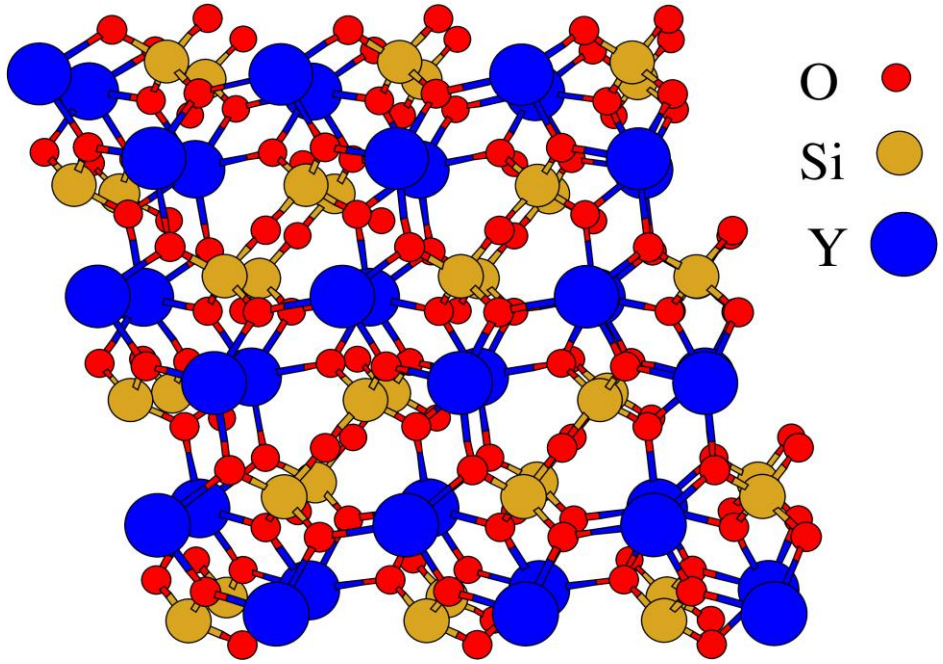

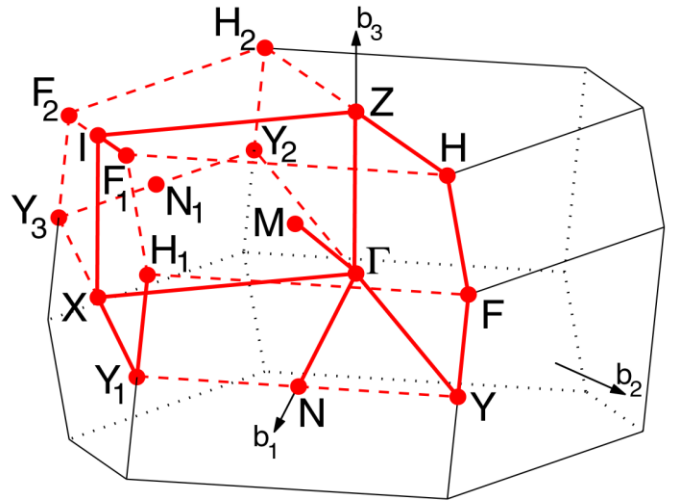

$MCLC_3$ path: Γ-Y-F-H-Z-I-X-Γ-Z|M-Γ-N|X-Y_1-H_1|I-F_1

[Setyawan & Curtarolo, DOI: 10.1016/j.commatsci.2010.05.010]

- Y2Si2O7 a=6.88, b=8.98, c=4.72,
- **Yb2Si2O7 a=6.82, b=9.01, c=4.76. Very close to above values**
- Both in monoclinic system, space group C2/m
- **Atomic structure from OQMD.**

S. Hao, R. Oleksak, O. Dorgan, M. Gao, Acta Materialia, 258 (2023), 119225

$Y_2Si_2O_7$ Phonon Dispersion and partial DOS

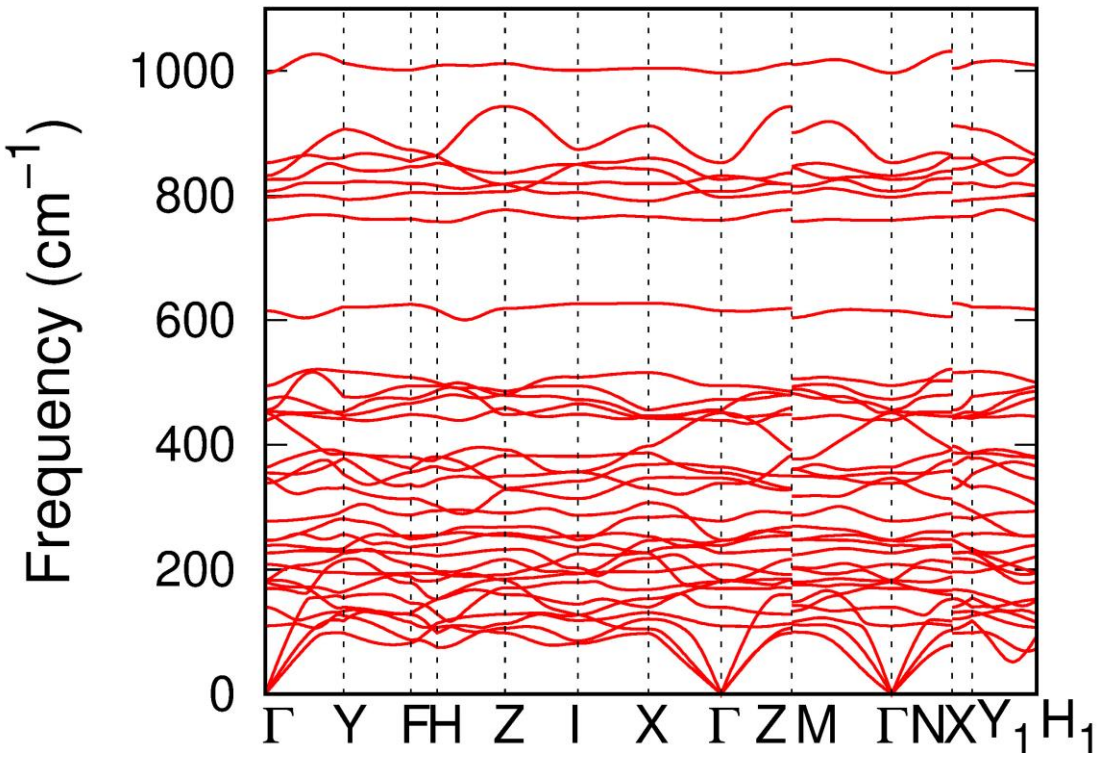

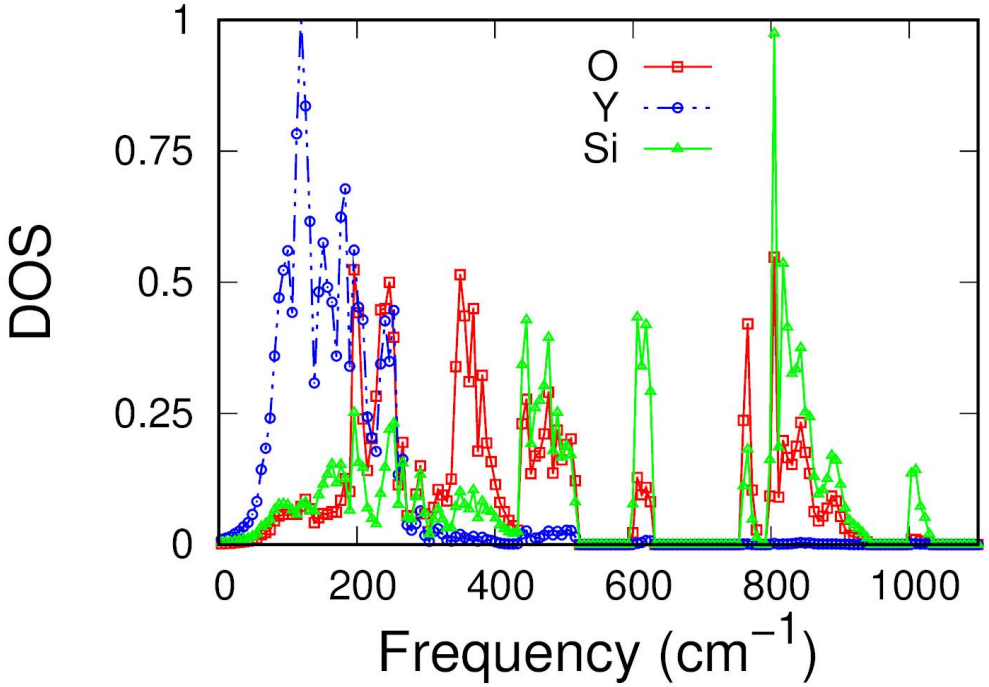

$$D_{ij}^{\alpha\beta}(\vec{q}) = \frac{1}{\sqrt{m_i m_j}} \sum_{l'} \Phi_{l_i l'_j}^{\alpha\beta} e^{i\vec{q}R_{l'}}$$

- Phonon dispersion: Y case
- Y contributes to low frequencies.
- O and Si for high frequencies

[14] L. Chaput, A. Togo, I. Tanaka, and G. Hug, Phonon-phonon interactions in transition metals, Phys. Rev. B 84 (2011) 094302.

$Yb_2Si_2O_7$ Phonon Dispersion and partial DOS

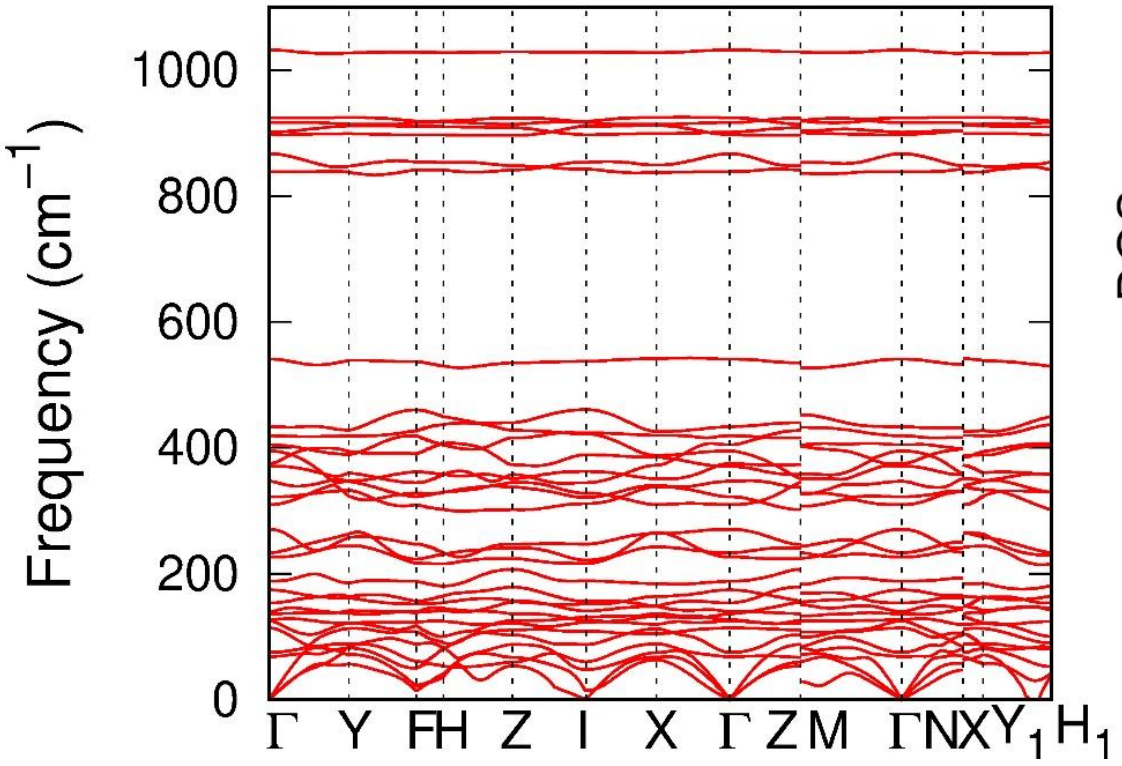

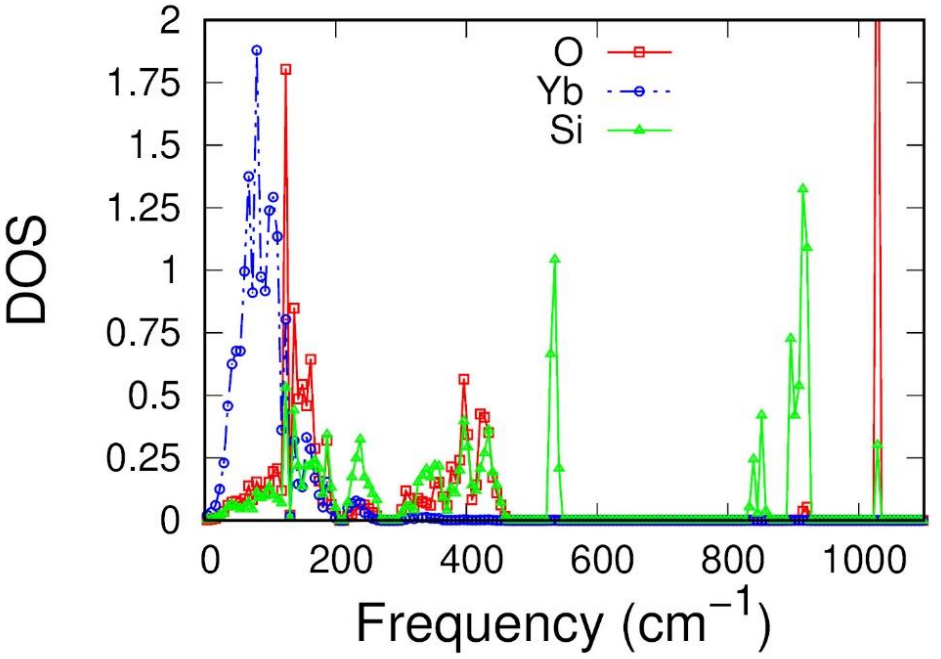

- Similar shape to Y2Si2O7 due to the same atomic structure.
- Yb frequencies are even lower than those of Y due to the heavier atomic mass.
- O and Si for high frequencies: Local vibrational modes.

S. Hao, R. Oleksak, O. Dorgan, M. Gao, Acta Materialia, 258 (2023), 119225

Lattice Thermal Conductivity: Methods

$$\kappa_i = \frac{1}{3} C_i T^3 \left\{ \int_0^{\Theta_i/T} \frac{\tau_c^i(x) x^4 e^x}{(e^x-1)^2} dx + \frac{\left[\int_0^{\Theta_i/T} \frac{\tau_c^i(x) x^4 e^x}{\tau_N^i (e^x-1)^2} dx \right]^2}{\int_0^{\Theta_i/T} \frac{\tau_c^i(x) x^4 e^x}{\tau_N^i \tau_U^i (e^x-1)^2} dx} \right\}$$

$$\frac{1}{\tau_N^{LA}(x)} = \frac{k_B{}^5 \gamma_{LA}{}^2 V}{M\hbar^4 v_{LA}{}^5} x^2 T^5$$

$$\frac{1}{\tau_N^{TA/TA'}(x)} = \frac{k_B{}^5 \gamma_{TA/TA'}{}^2 V}{M\hbar^4 v_{TA/TA'}{}^5} x T^5$$

$$\frac{1}{\tau_U^i(x)} = \frac{k_B{}^2 \gamma_i^2}{M\hbar v_i^2 \Theta_i} x^2 T^3 e^{-\theta_i/3T}$$

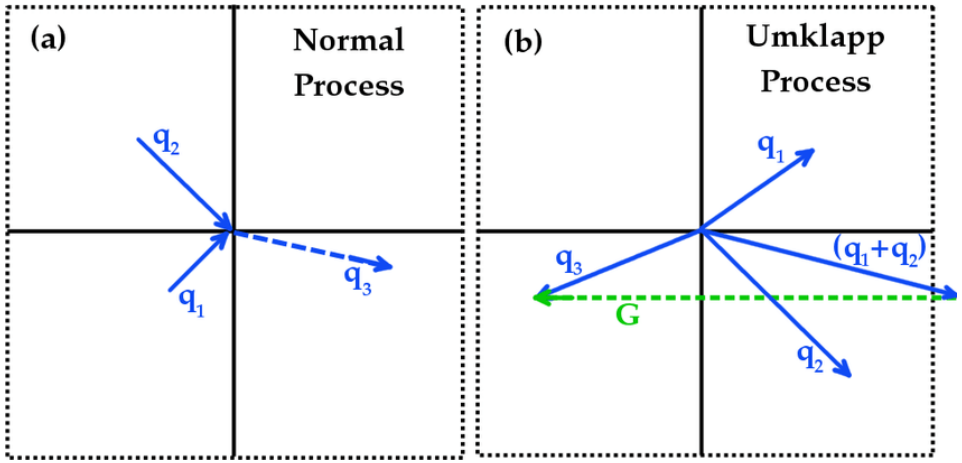

- Debye-Callaway model
- normal phonon scattering
- Umklapp phonon–phonon scattering
- Not considered: impurity, boundary scatterings.

S. Hao, R. Oleksak, O. Dorgan, M. Gao, Acta Materialia, 258 (2023), 119225

Lattice Thermal Conductivity: Results

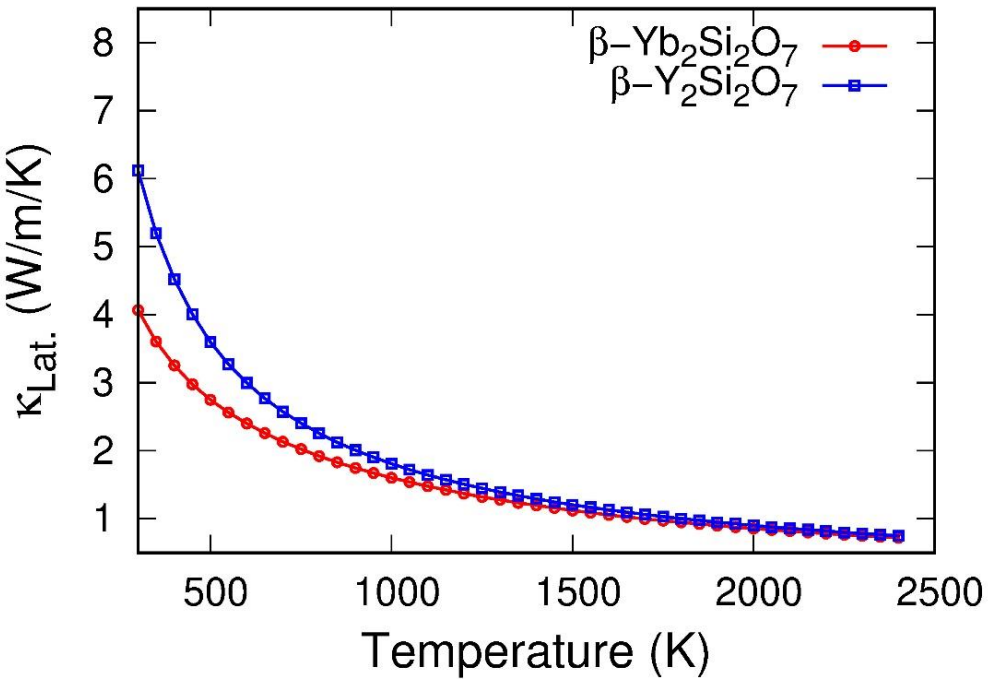

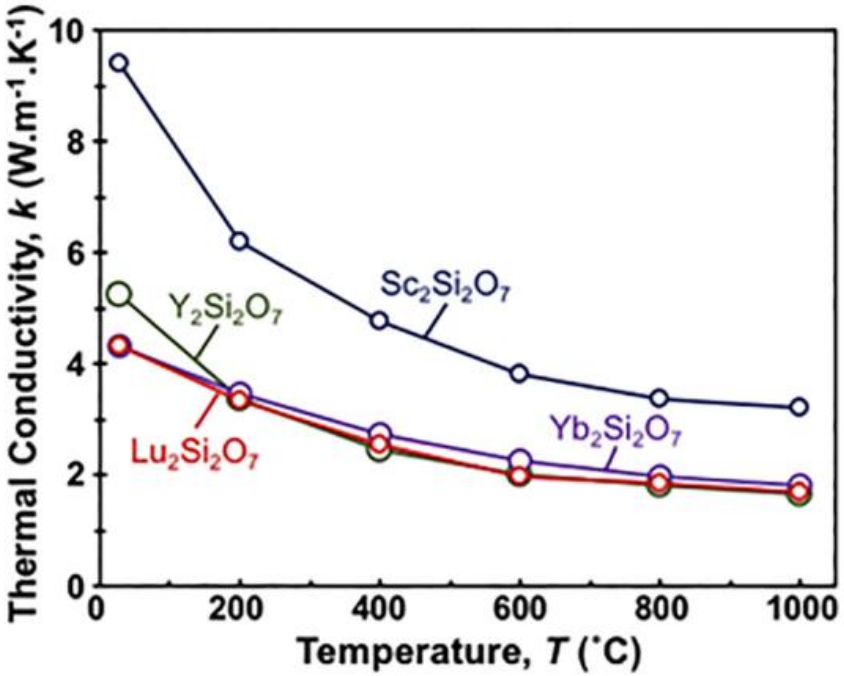

The lattice thermal conductivities of Yb case are lower than those of Y case.

Physical reasons: Heavier Yb atoms induce lower frequencies, thus lower Debye temperatures and slower phonon group velocities. Yb case has larger Gruneisen parameters suggesting stronger anharmonicity than Y case. All these contribute to lowering lattice thermal conductivities.

Z. Tian, L. Zheng, Z. Li, J. Li, J. Wang, J. Eur. Ceram. Soc. 36 (2016) 2813.

Cluster Expansion for mixing of $Yb_2Si_2O_7$ and $Y_2Si_2O_7$

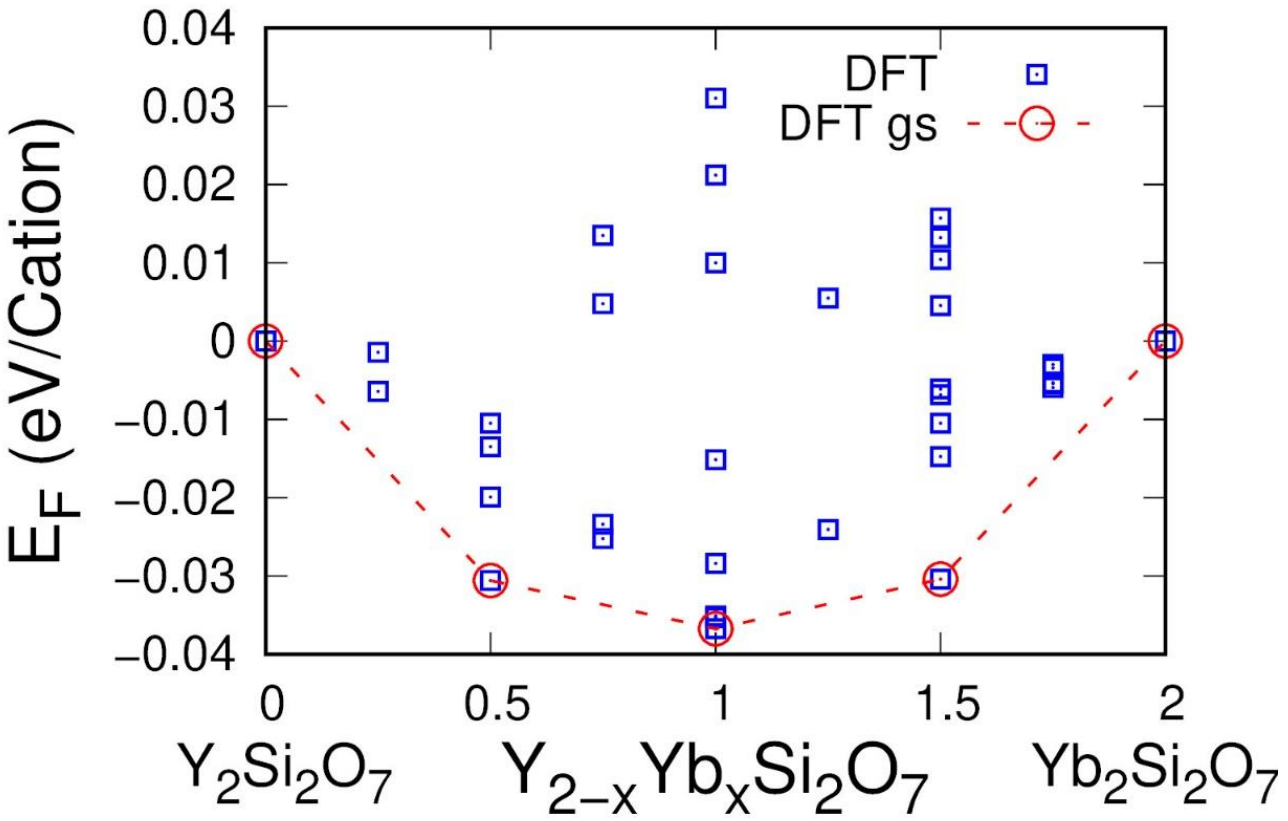

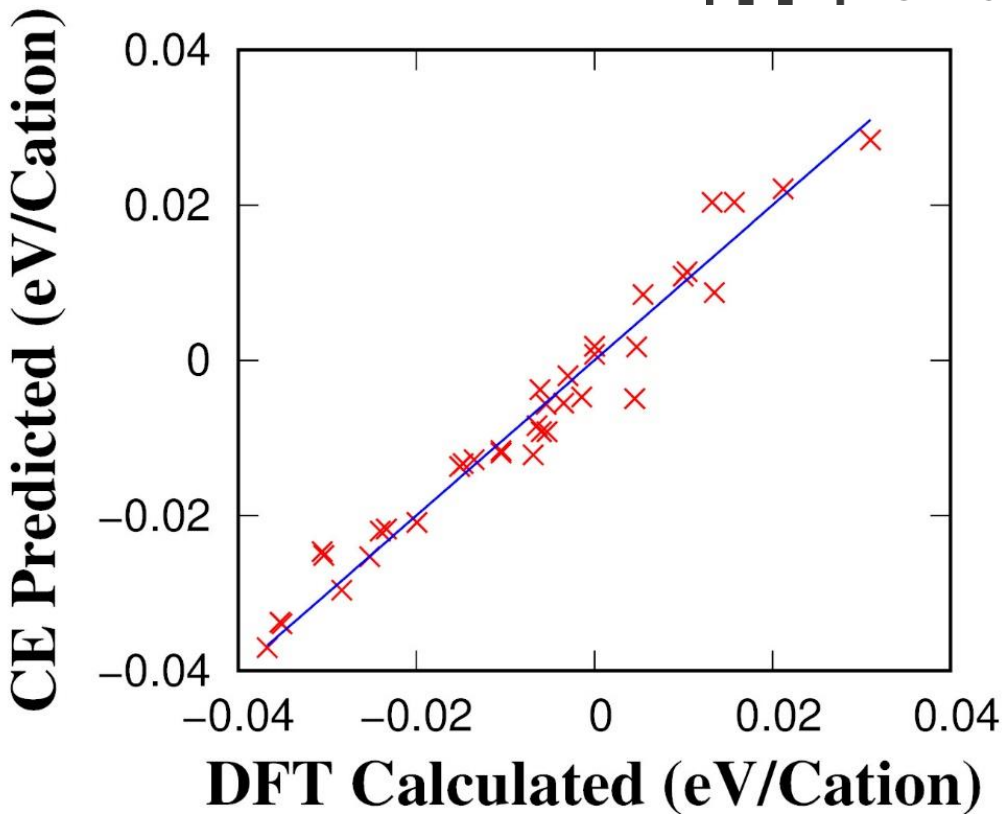

$$E(\sigma) = \sum_{\alpha} m_{\alpha} J_{\alpha} \langle \Pi \sigma_i \rangle$$

Accurate cluster expansion predicts three stable ordered compounds, $Y_{1.5}Yb_{0.5}Si_2O_7$, $Y_1Yb_1Si_2O_7$, $Y_{0.5}Yb_{1.5}Si_2O_7$.

S. Hao, R. Oleksak, O. Dorgan, M. Gao, Acta Materialia, 258 (2023), 119225

Predicted New Ordered Structures

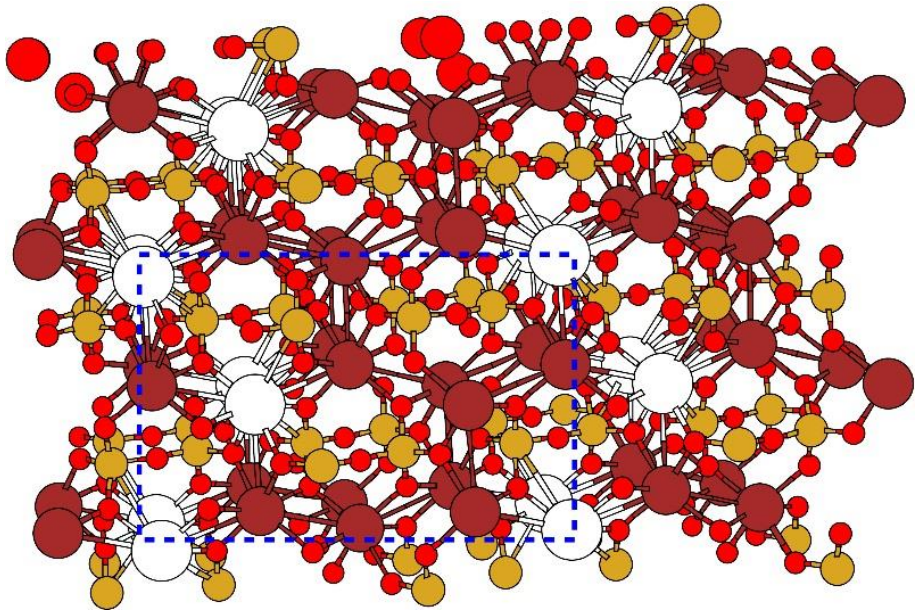

$Y_{1.5}Yb_{0.5}Si_2O_7$
Space group : $P2_1$

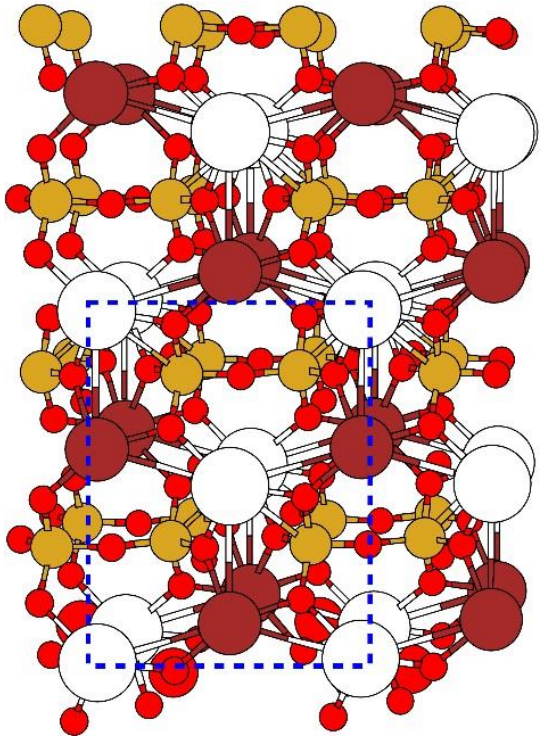

$Y_1Yb_1Si_2O_7$
Space group : C2

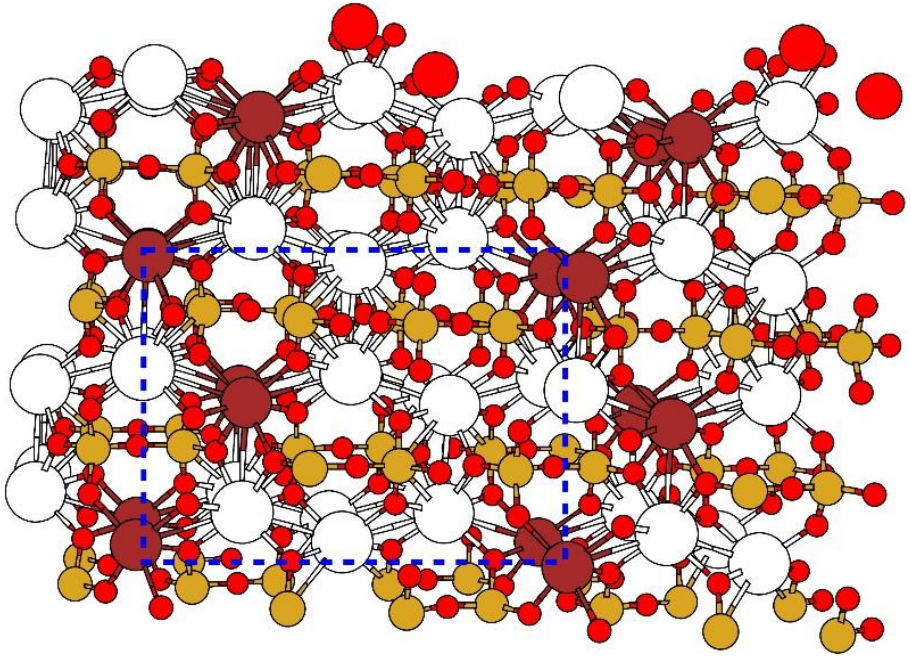

$Y_{0.5}Yb_{1.5}Si_2O_7$
Space group : $P2_1$

S. Hao, R. Oleksak, O. Dorgan, M. Gao, Acta Materialia, 258 (2023), 119225

Order Disorder Transation Temperatures

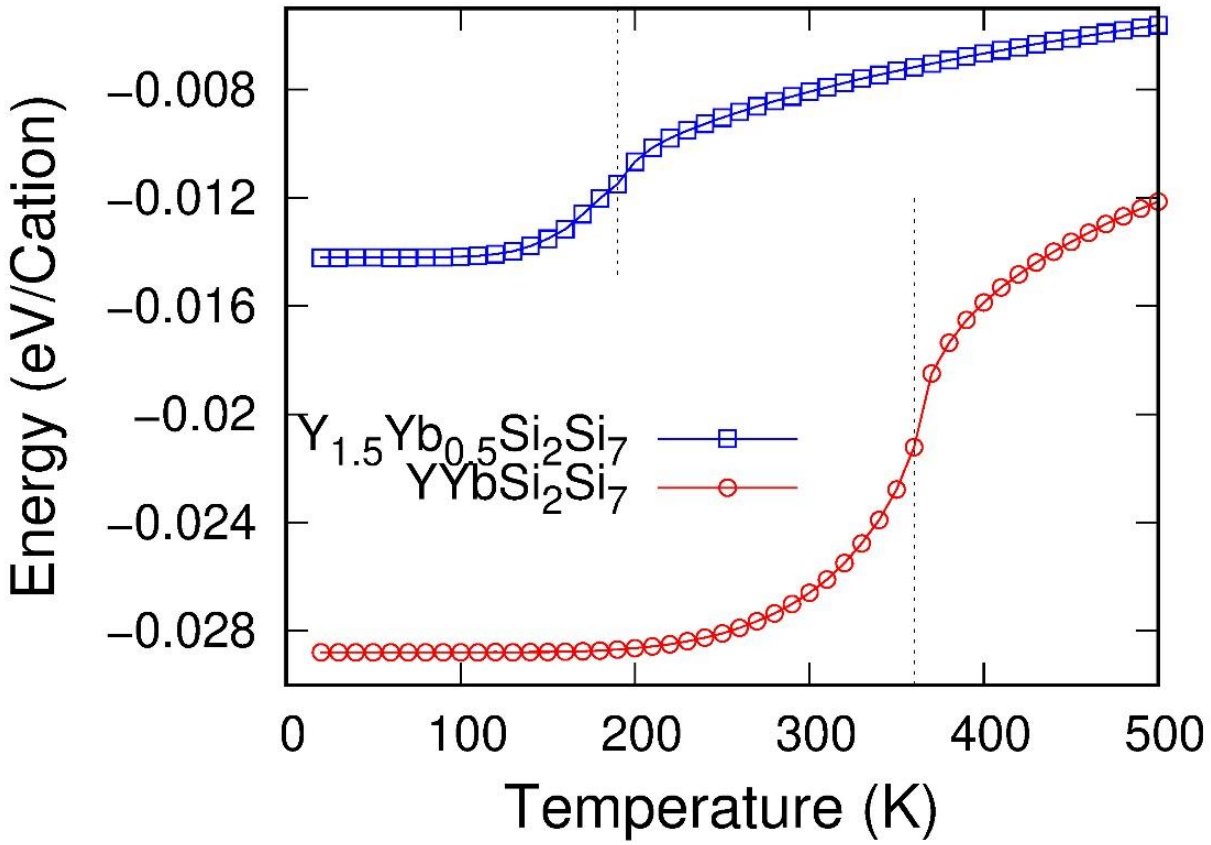

Canonical Monte Carlo simulation for YYbSi2O7 based on the spin- polarized cluster expansion.

Order disorder transition temperature: 360 K.

Novel ordered stable structure prediction !!

Suggest experimental confirmation.

S. Hao, R. Oleksak, O. Dorgan, M. Gao, Acta Materialia, 258 (2023), 119225

$YYbSi_2O_7$ Phonon Dispersion and partial DOS

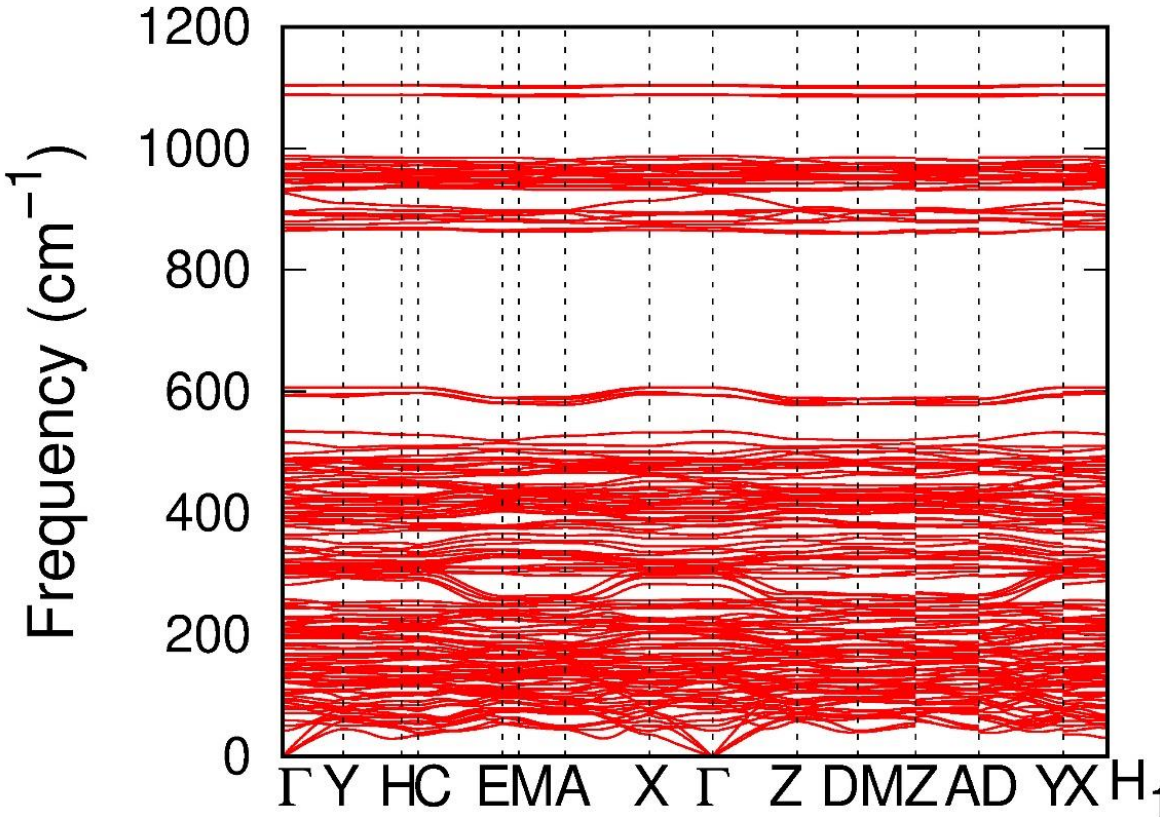

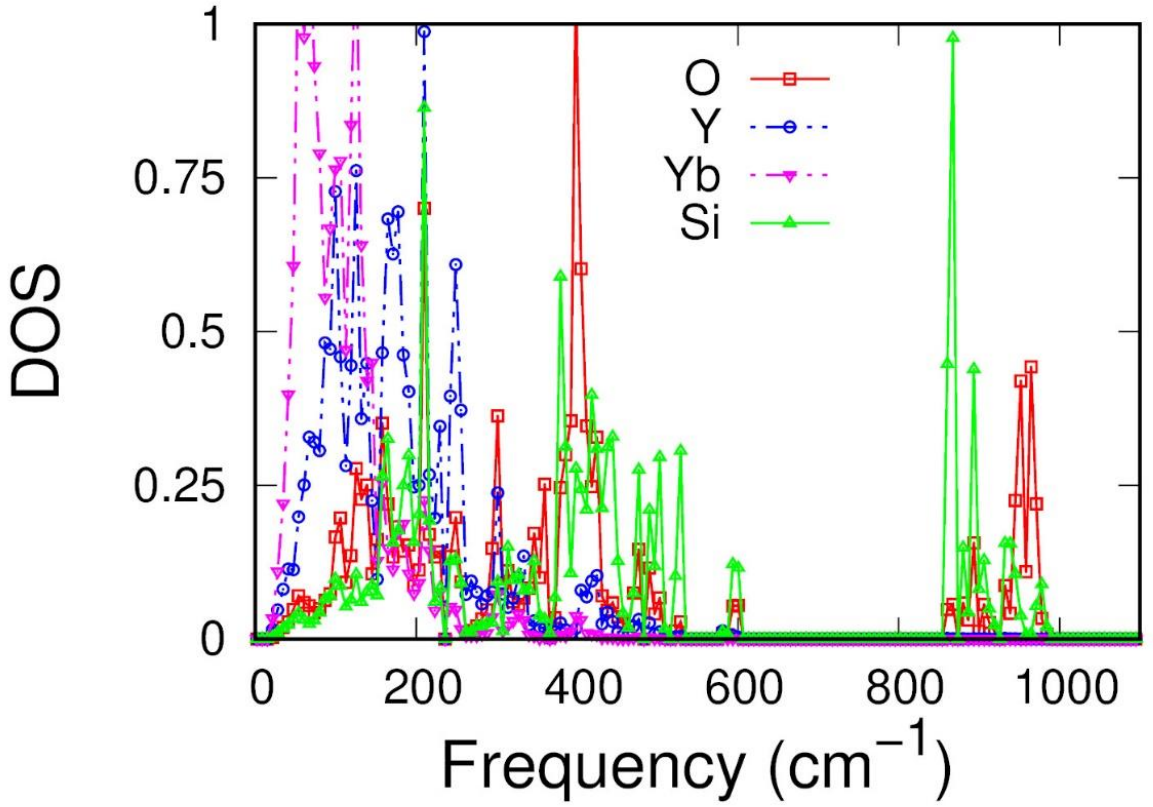

Special quasi-random structure for the solid solution of $Y_1Yb_1Si_2O_7$

S. Hao, R. Oleksak, O. Dorgan, M. Gao, Acta Materialia, 258 (2023), 119225

$YYbSi_2O_7$ Lattice Thermal Conductivity

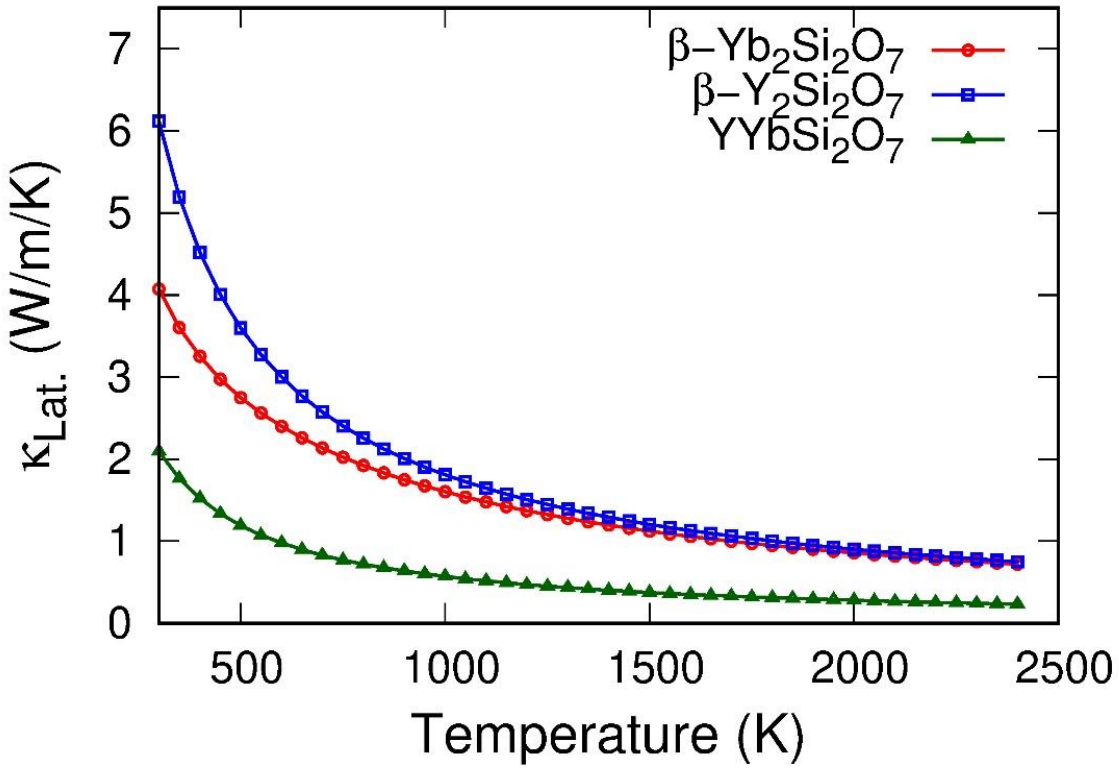

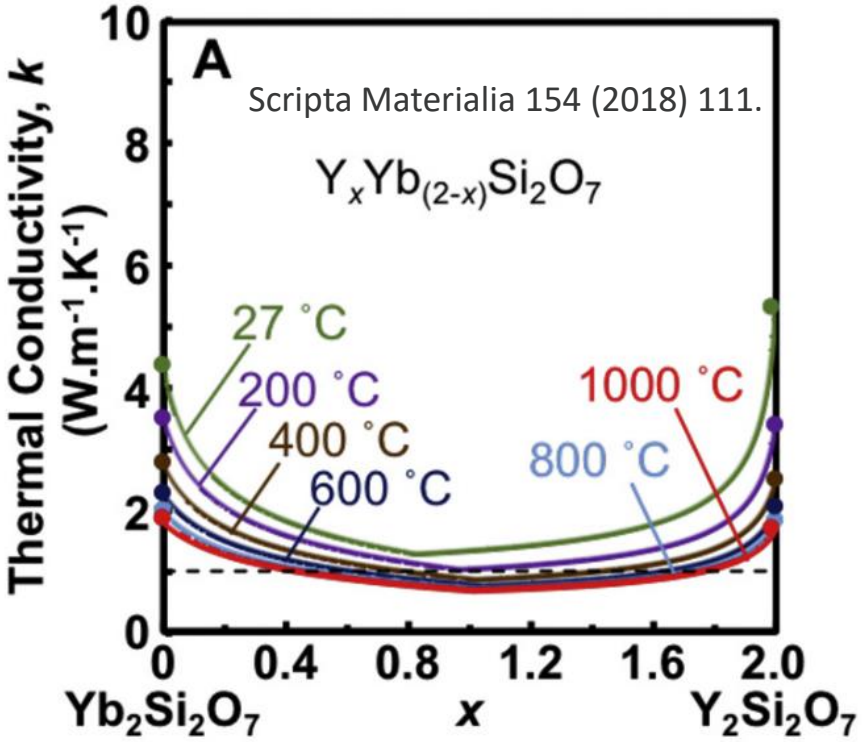

- $Y_1Yb_1Si_2O_7$ has even lower lattice thermal conductivity than both Y and Yb cases. Calculated results are slightly higher than literature.
- Physical reasons: disordered Y and Yb sublattice forming mass fluctuation and lattice distortion induce strong phonon scatterings.

S. Hao, R. Oleksak, O. Dorgan, M. Gao, Acta Materialia, 258 (2023), 119225

More Solid Solutions: Phonon Dispersions

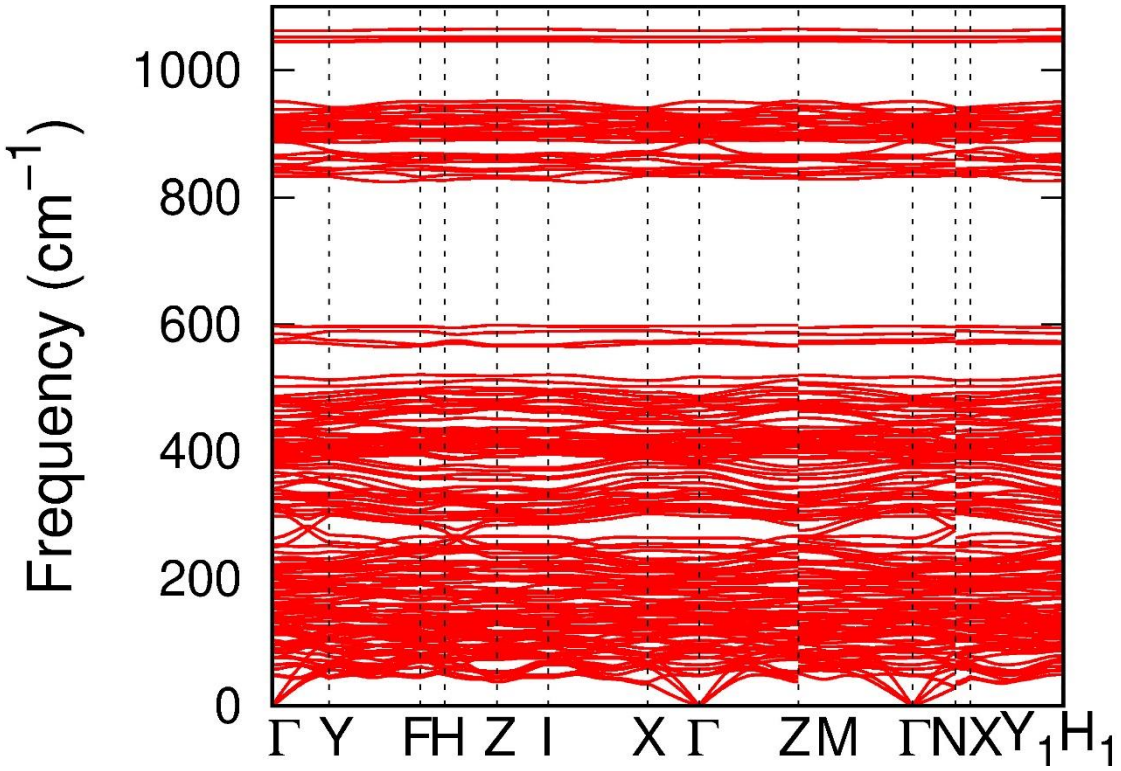

$Er_{1/4}Lu_{1/4}Y_{3/4}Yb_{3/4}Si_2O_7$

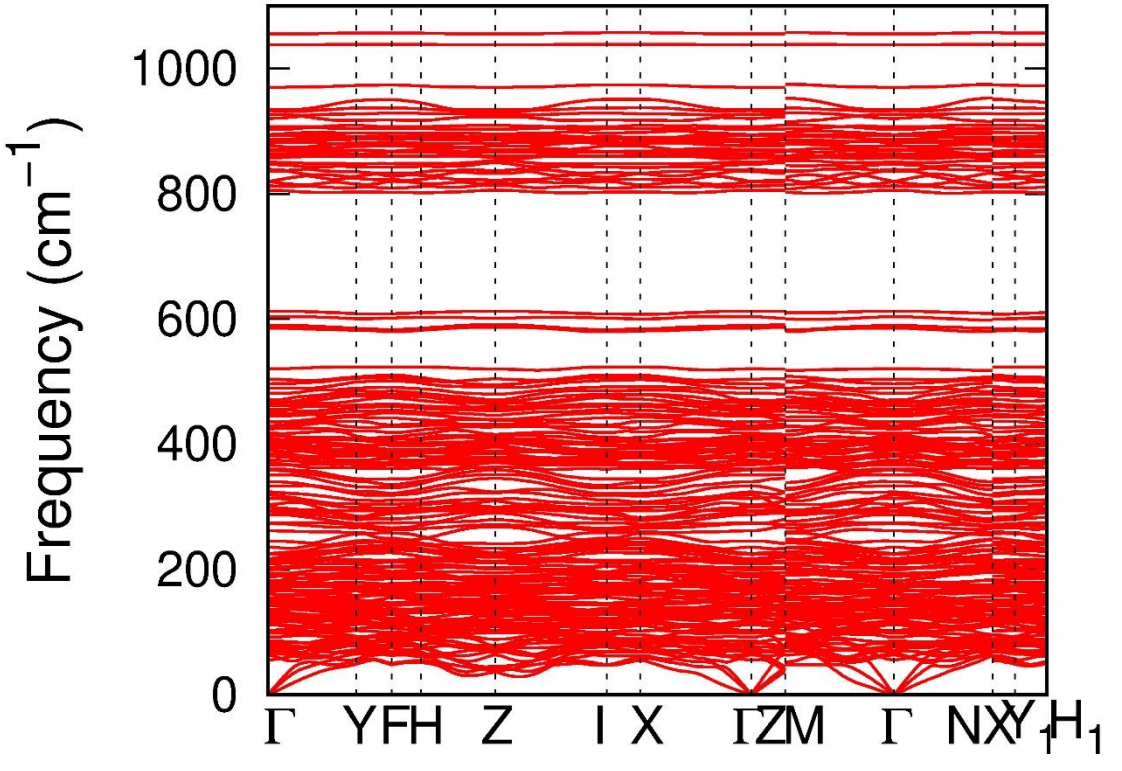

$La_{1/4}Ce_{1/4}Er_{1/4}Lu_{1/4}Y_{1/2}Yb_{1/2}Si_2O_7$

S. Hao, R. Oleksak, O. Dorgan, M. Gao, Acta Materialia, 258 (2023), 119225

Thermal Expansion: Quasi-harmonic Approximation

$F_{total}(T,V) = E_{DFT}(V) + F_{vib}(T,V)$.

$$F_{\text{vib}} = k_B T \int d\nu\, g(\nu) \ln\left[2 \sinh \frac{h\nu}{2k_B T}\right],$$

$$\beta = \frac{1}{V}\frac{\partial V}{\partial T}$$

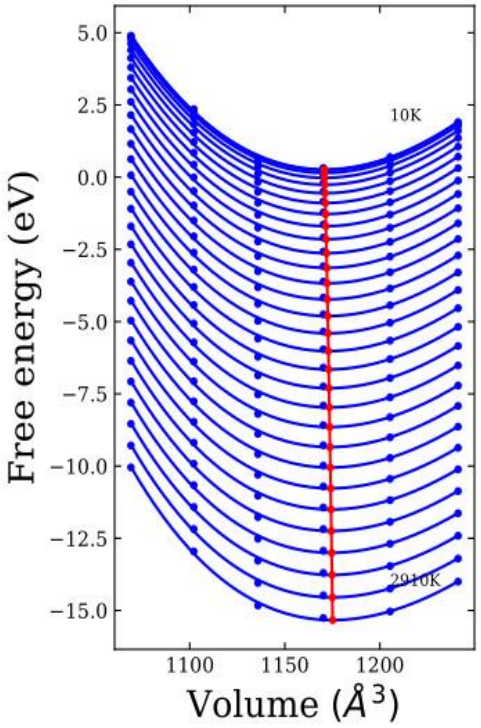

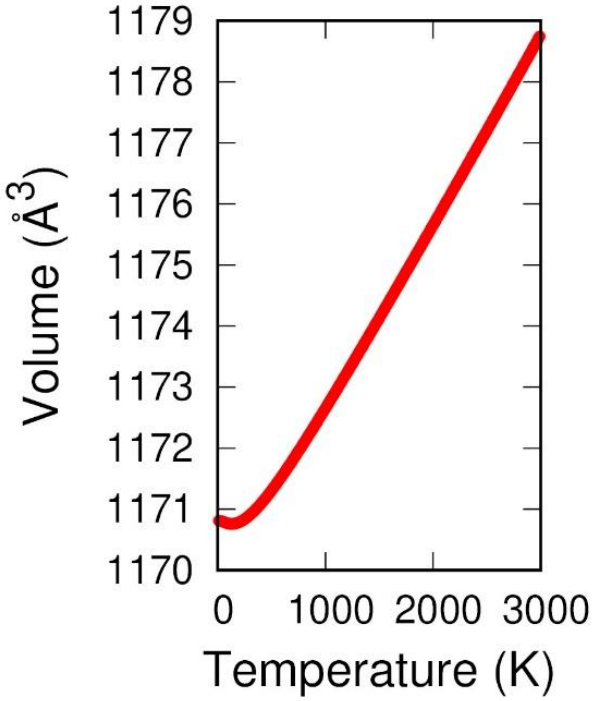

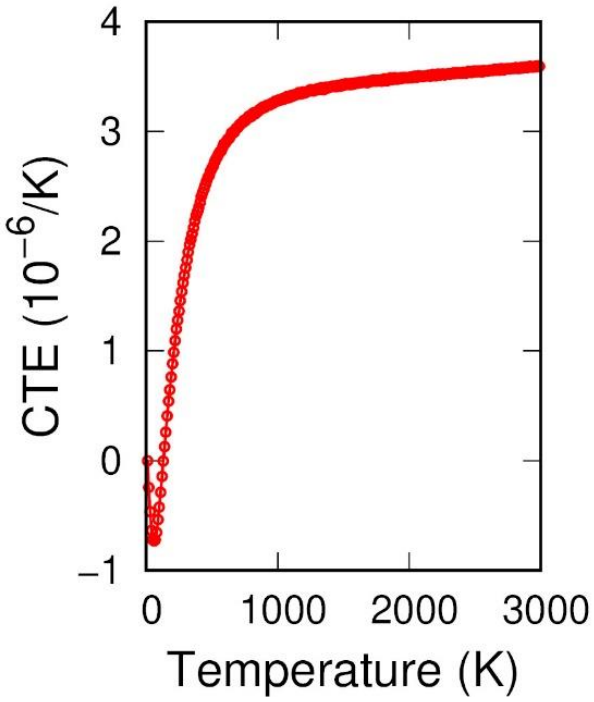

CTE $Y_2Si_2O_7$:

3.4×10^{-6} K^{-1} at high T.

S. Hao, R. Oleksak, O. Dorgan, M. Gao, Acta Materialia, 258 (2023), 119225

Free Energy and Volume as a Function of T

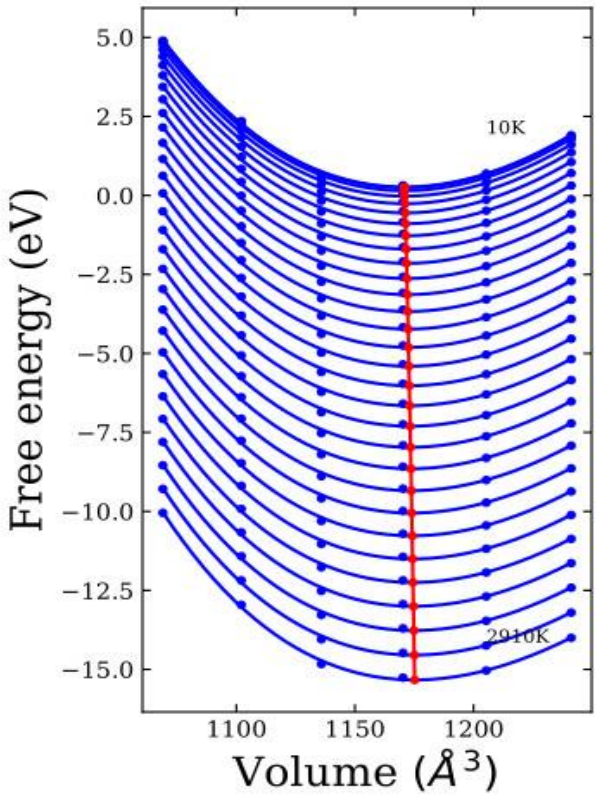

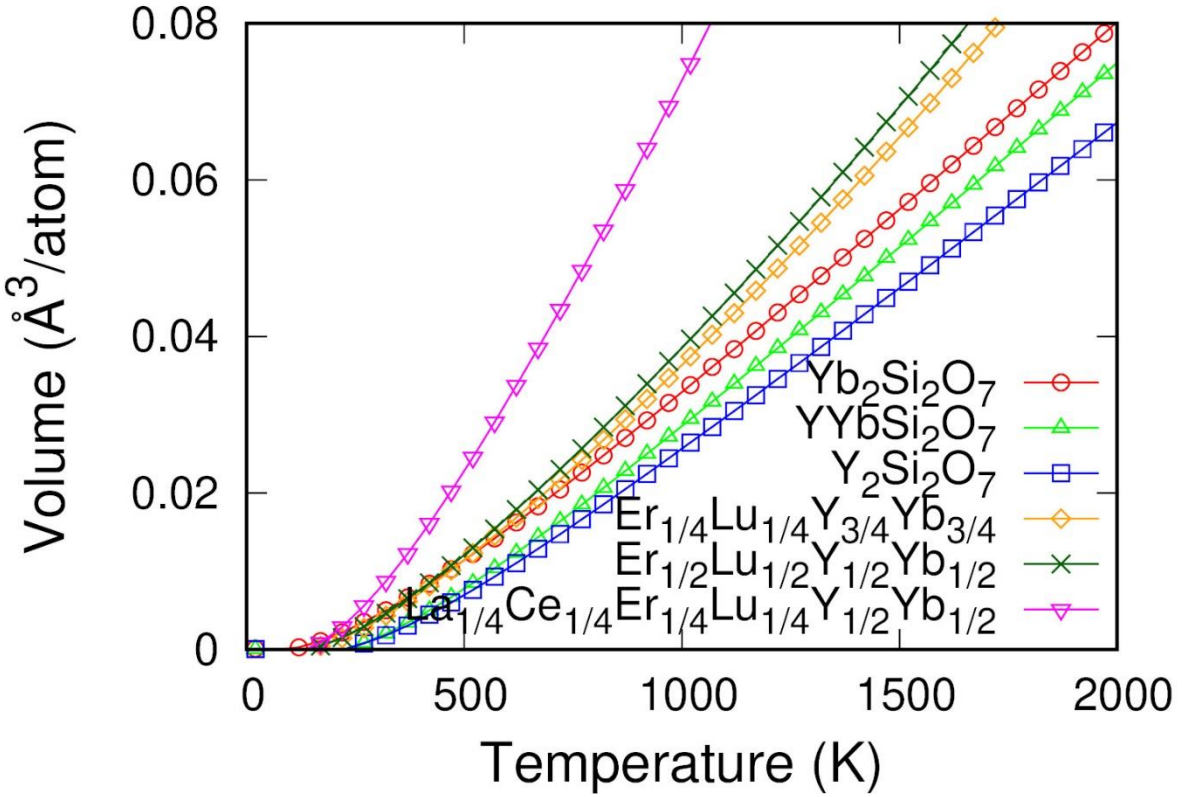

- Phonon energy → Free energy map as a function of V and T F(V,T) → Volume as a function V(T).

S. Hao, R. Oleksak, O. Dorgan, M. Gao, Acta Materialia, 258 (2023), 119225

Comparison of Coefficients of Thermal Expansion

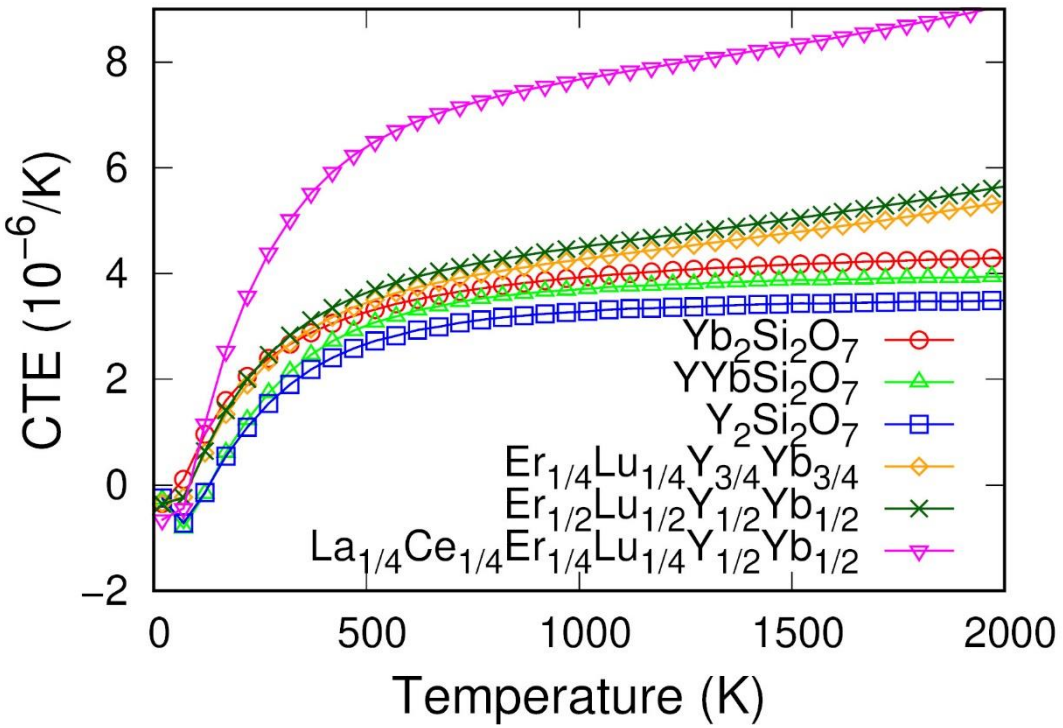

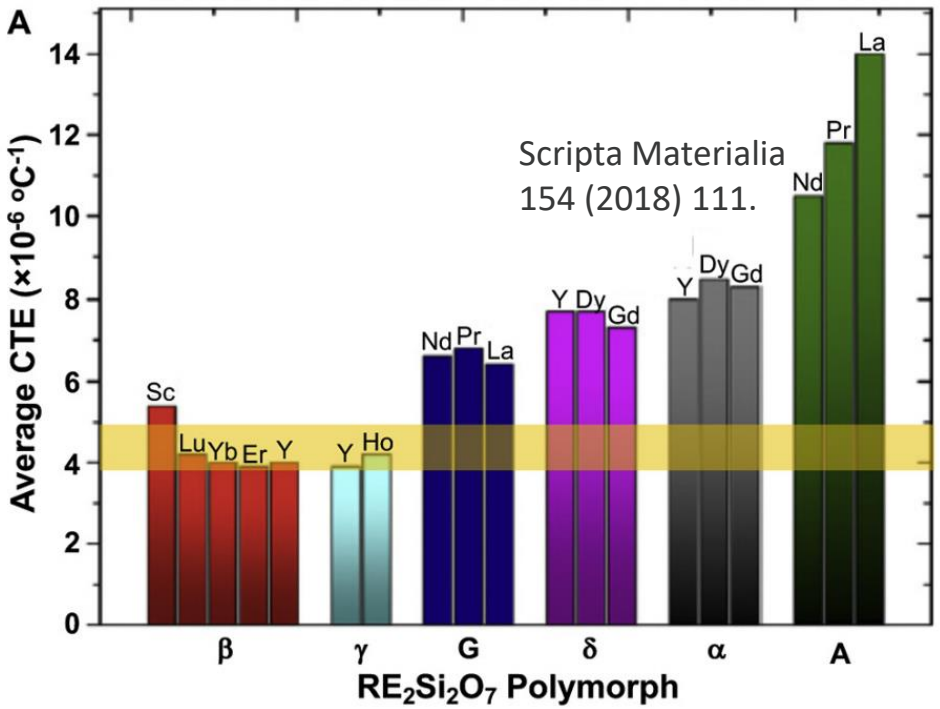

$$S_{Conf} = -R\frac{N_A}{N}\sum_{i_A}\frac{N_{a_i}}{N_A}\ln\frac{N_{ai}}{N_A}$$

- The coefficients of thermal expansion of $Y_1Yb_1Si_2O_7$ lie between Y and Yb, slightly higher than the average of Y and Yb.
- $Er_{1/4}Lu_{1/4}Y_{3/4}Yb_{3/4}$ exhibits good match with SiC. $La_{1/4}Ce_{1/4}Er_{1/4}Lu_{1/4}Y_{1/2}Yb_{1/2}$ is much higher.
- Beside vibrational entropy, the configuration entropy is also considered due to randomness of Y and Yb in the sublattice.

Comparison of Lattice Thermal Conductivities

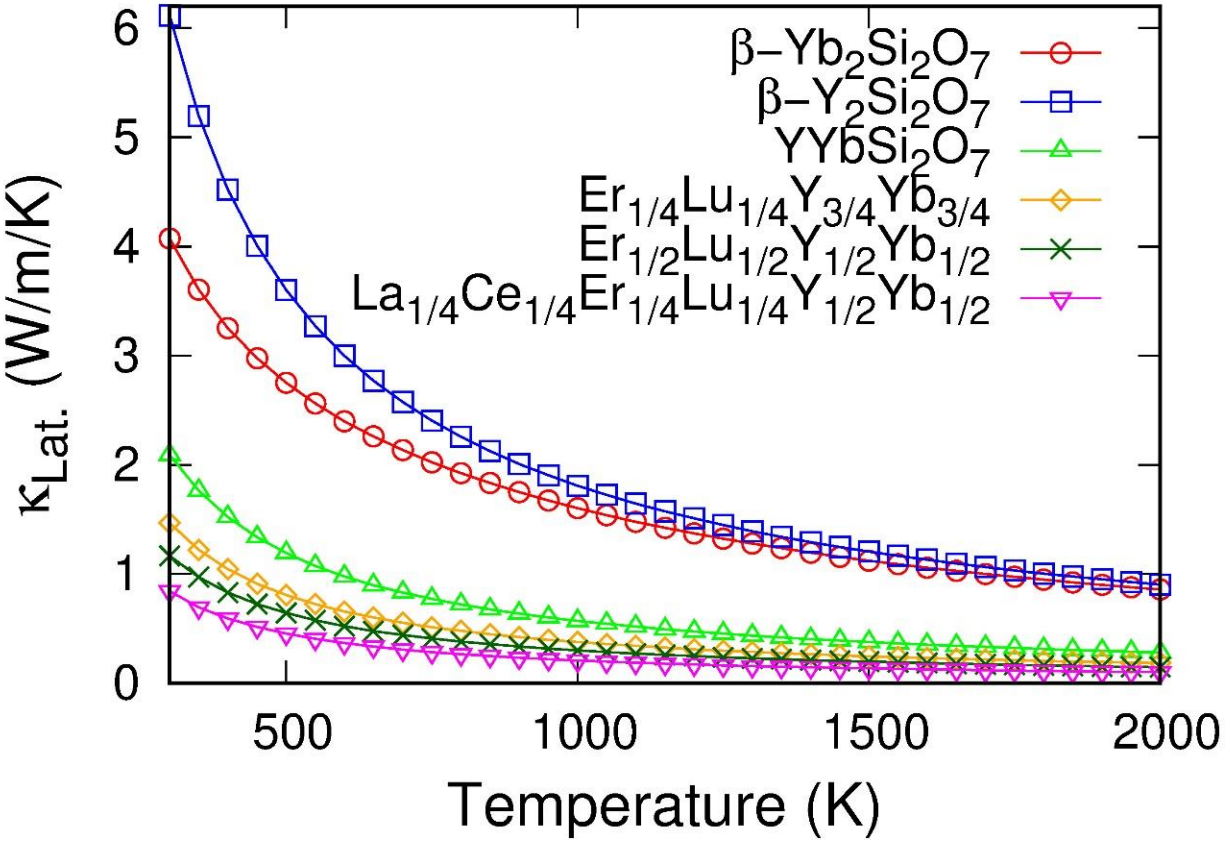

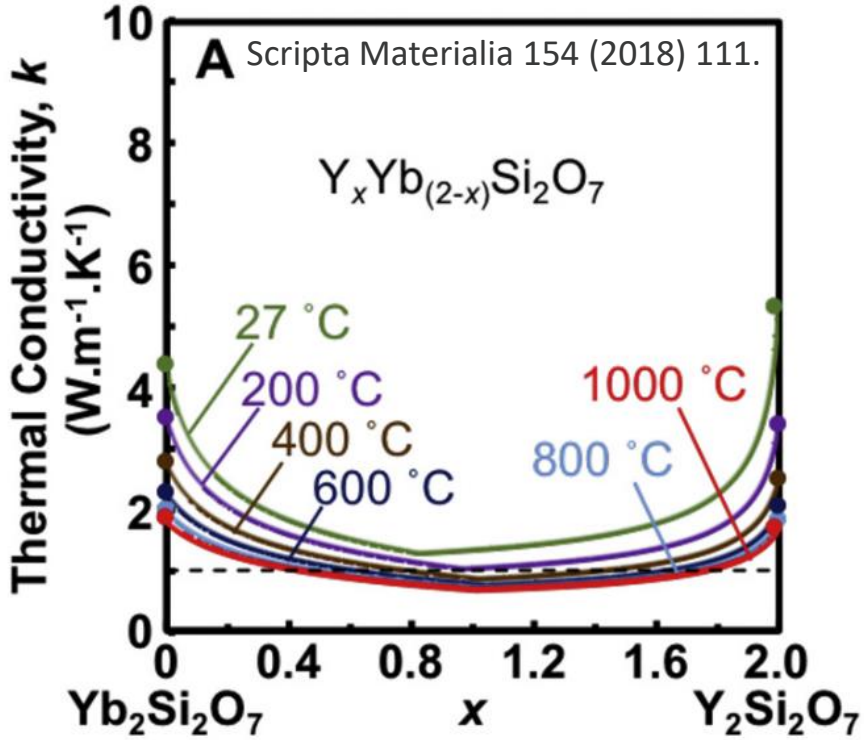

- The lattice thermal conductivity of $Yb_2Si_2O_7$, $Y_2Si_2O_7$, and $YYbSi_2O_7$ agree well with literature.
- $Er_{1/4}Lu_{1/4}Y_{3/4}Yb_{3/4}$ and $La_{1/4}Ce_{1/4}Er_{1/4}Lu_{1/4}Y_{1/2}Yb_{1/2}$ show even lower lattice thermal conductivity.

Mechanical Properties of $Yb_2Si_2O_7$

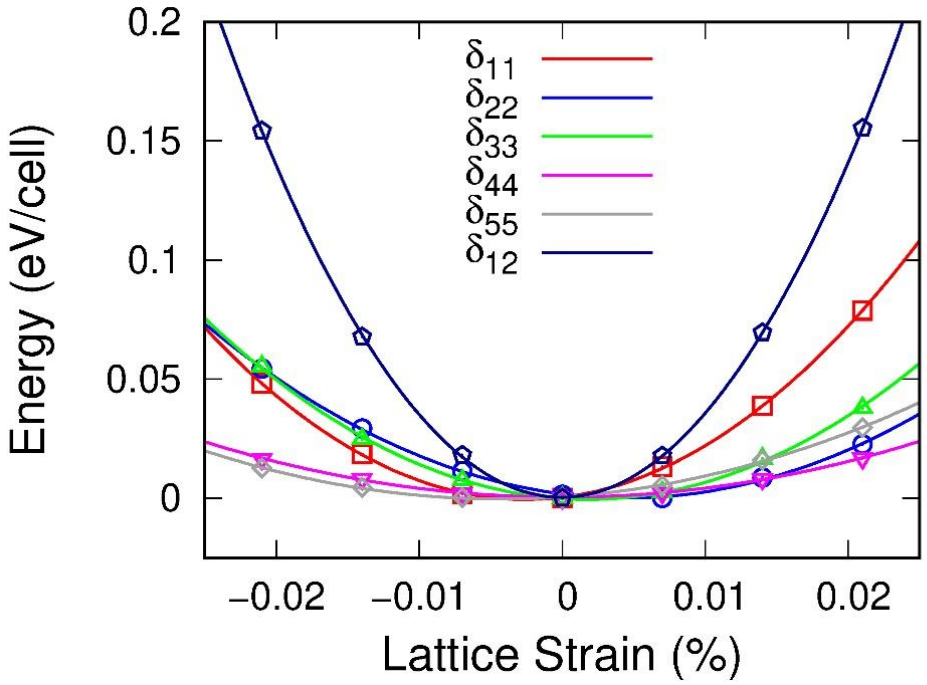

Agree with Literature 162GPa

62GPa

Scripta Materialia 154 (2018) 111.

Yb_2S
298.
91.4
110.
0.0
-17.3
0.0

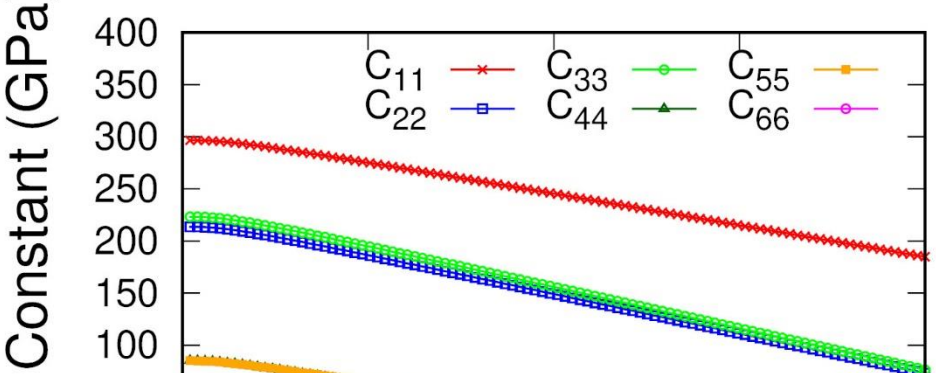

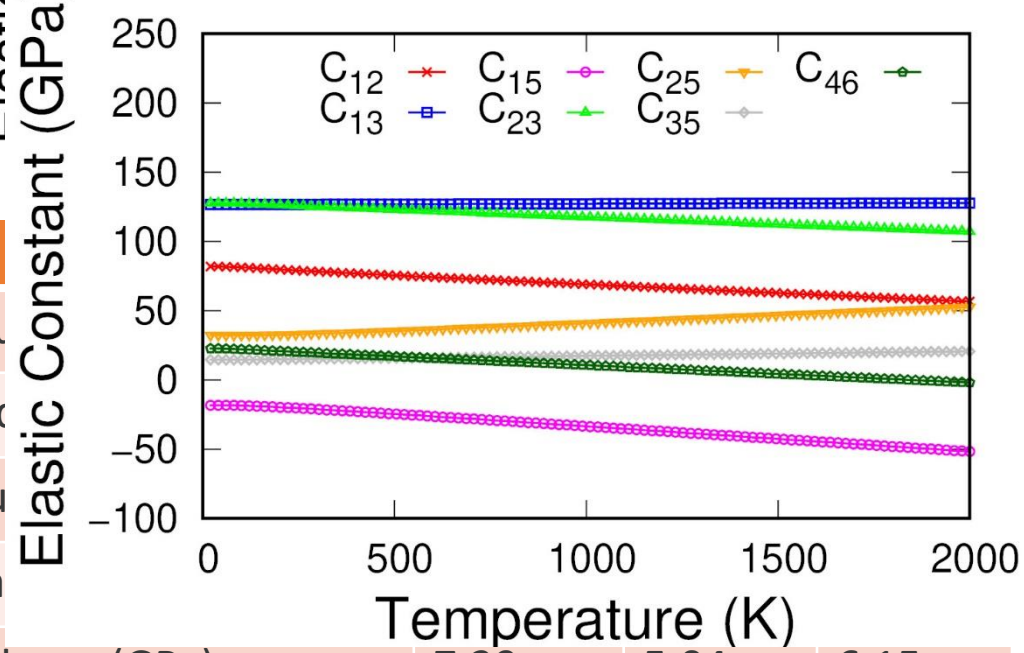

Mechanical			
Bulk Modulu			
Young's Mod			
Shear Modu			
Poisson's Ra			
Vickers Hardness (GPa)	7.29	5.04	6.15

S. Hao, R. Oleksak, O. Dorgan, M. Gao, Acta Materialia, 258 (2023), 119225

Mechanical Properties of $Y_2Si_2O_7$

$Y_2Si_2O_7$ Stiffness Tensor (GPa)					
272.6	78.4	96.9	0.0	-15.3	0.0
78.4	190.8	107.4	0.0	32.4	0.0
96.9	107.4	184.9	0.0	13.8	0.0
0.0	0.0	0.0	75.5	0.0	20.2
-15.3	32.4	13.8	0.0	77.2	0.0
0.0	0.0	0.0	20.2	0.0	52.2

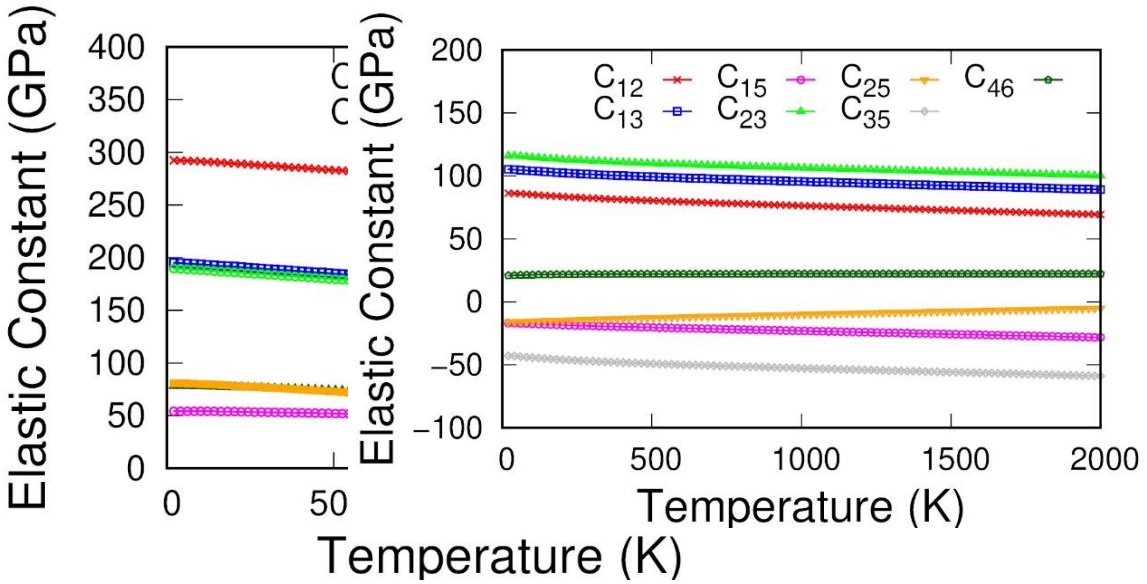

Agree with Literature 170GPa →

65GPa →

Scripta Materialia 154 (2018) 111.

Mechanical Properties	Voigt	Reuss	Hill
Bulk Modulus B (GPa)	134.9	130.2	132.5
Young's Modulus E(GPa)	168.8	145.7	157.3
Shear Modulus G(GPa)	65.4	55.5	60.4
Poisson's Ratio v	0.29	0.31	0.30
Vickers Hardness (GPa)	6.83	4.69	5.74

S. Hao, R. Oleksak, O. Dorgan, M. Gao, Acta Materialia, 258 (2023), 119225

Mechanical Properties of $YYbSi_2O_7$

$YYbSi_2O_7$ Stiffness Tensor (GPa)					
258.4	74.4	91.8	0.0	-14.3	0.0
74.4	184.6	99.9	0.0	25.5	0.0
91.8	99.9	183.6	0.0	8.53	0.0
0.0	0.0	0.0	75.4	0.0	15.5
-14.3	25.5	8.53	0.0	75.1	0.0
0.0	0.0	0.0	15.5	0.0	49.4

Mechanical Properties	Voigt	Reuss	Hill
Bulk Modulus B (GPa)	128.7	125.8	127.3
Young's Modulus E(GPa)	164.7	147.3	156.1
Shear Modulus G(GPa)	64.0	56.4	60.2
Poisson's Ratio v	0.29	0.31	0.30
Vickers Hardness (GPa)	7.00	5.24	6.11

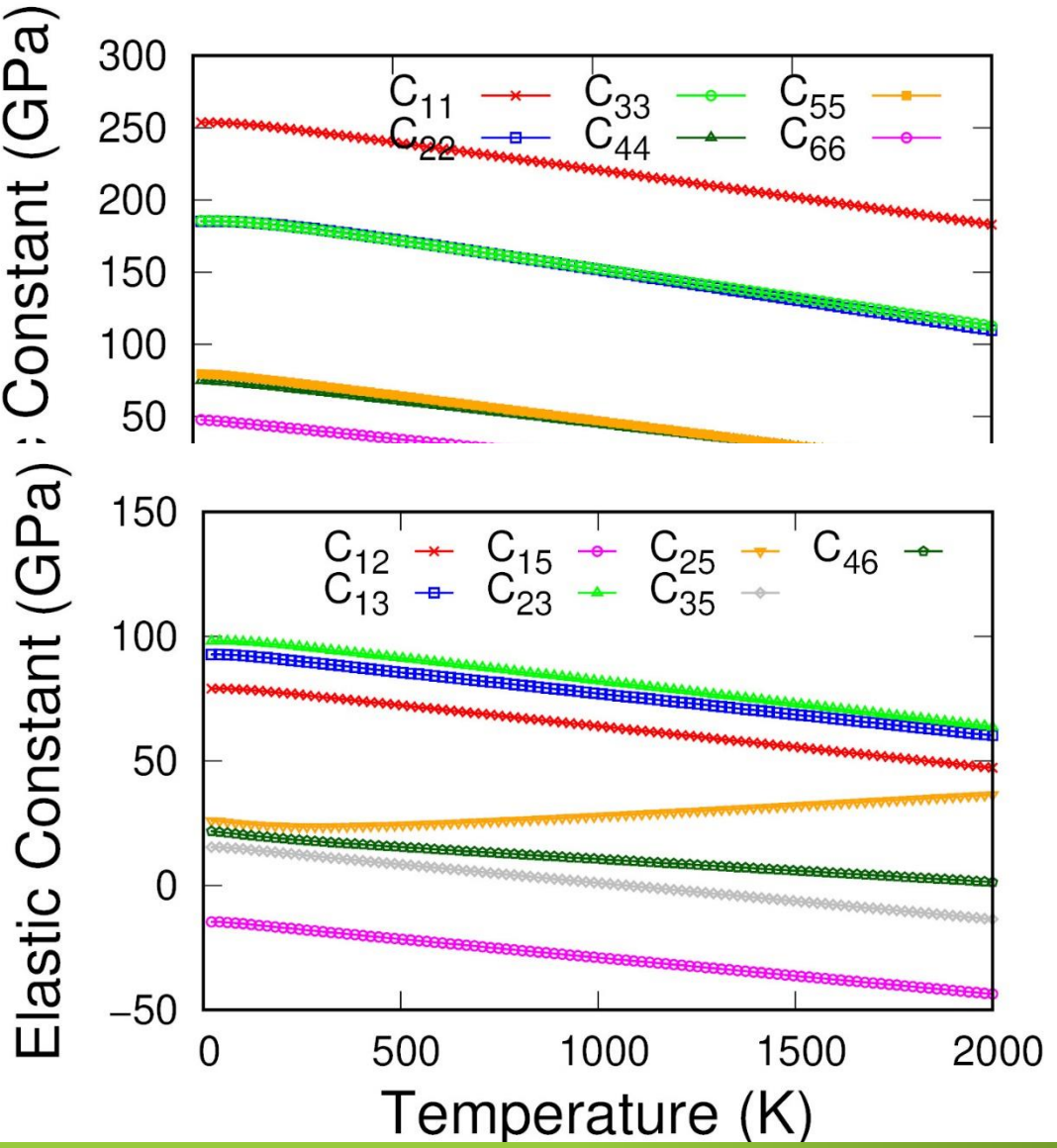

S. Hao, R. Oleksak, O. Dorgan, M. Gao, Acta Materialia, 258 (2023), 119225

$Er_{1/2}Lu_{1/2}Y_{1/2}Yb_{1/2}Si_2O_7$

$Er_{1/4}Lu_{1/4}Y_{3/4}Yb_{3/4}Si_2O_7$ Stiffness Tensor (GPa)					
201.7	101.7	115.5		-5.1	
101.7	204.1	104.7		39.1	
115.5	104.7	277.1		-16.6	
			65.8		26.1
-5.1	39.1	-16.6		93.4	
			26.1		71.6

Mechanical Properties	Voigt	Reuss	Hill
Bulk Modulus B (GPa)	147.4	142.4	144.9
Young's Modulus E(GPa)	181.8	155.7	168.9
Shear Modulus G(GPa)	70.2	59.1	64.7
Poisson's Ratio v	0.29	0.32	0.31
Vickers Hardness (GPa)	7.05	4.73	5.87

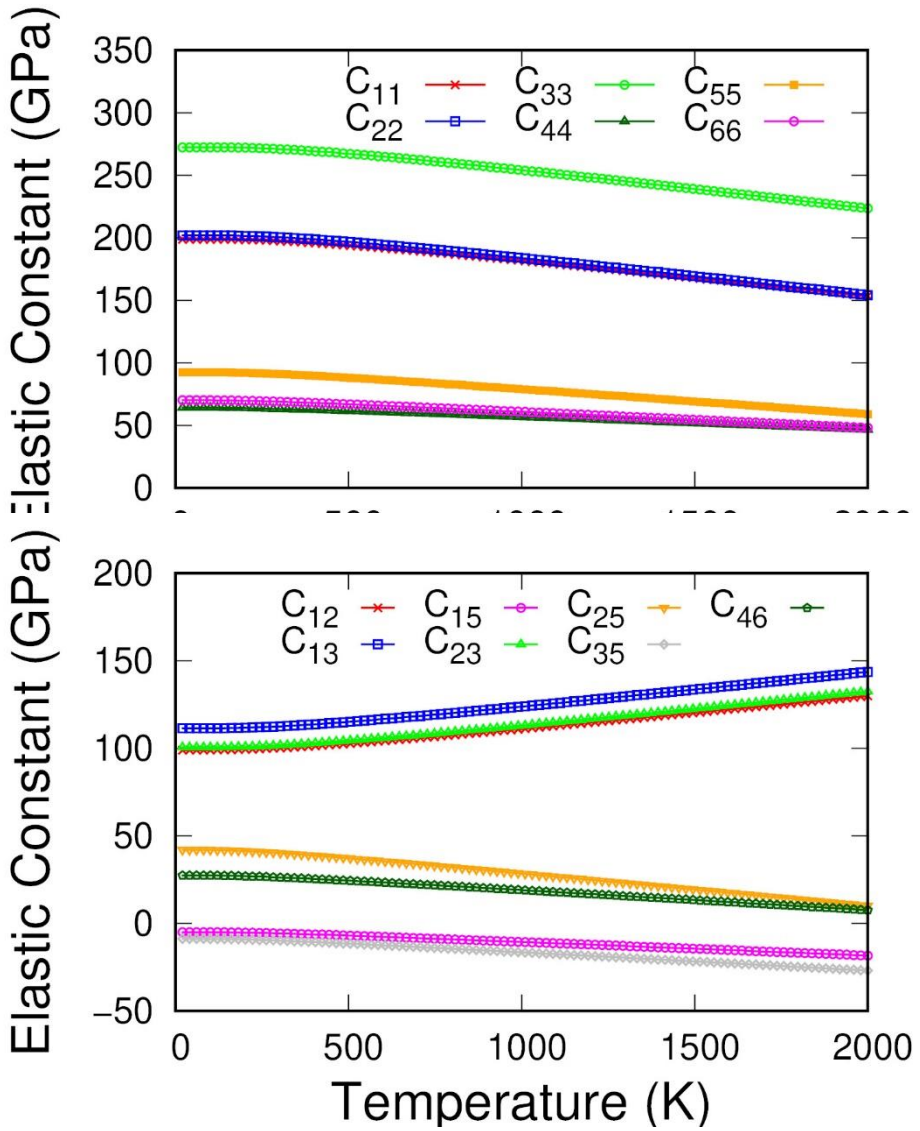

S. Hao, R. Oleksak, O. Dorgan, M. Gao, Acta Materialia, 258 (2023), 119225

$La_{1/4}Ce_{1/4}Er_{1/4}Lu_{1/4}Y_{1/2}Yb_{1/2}Si_2O_7$

$Er_{1/4}Lu_{1/4}La_{1/4}Ce_{1/4}Y_{1/2}Yb_{1/2}Si_2O_7$ (GPa)					
173.8	86.9	104.4		-1.5	
86.9	178.5	92.9		-18.4	
104.4	92.9	268.8		13.7	
			58.1		-5.74
-1.5	-18.4	13.7	0.0	85.7	
			-5.74		57.8

Mechanical Properties	Voigt	Reuss	Hill
Bulk Modulus B (GPa)	132.2	125.6	128.9
Young's Modulus E(GPa)	162.6	143.1	152.9
Shear Modulus G(GPa)	62.8	54.6	58.7
Poisson's Ratio v	0.30	0.31	0.30
Vickers Hardness (GPa)	6.38	4.79	5.58

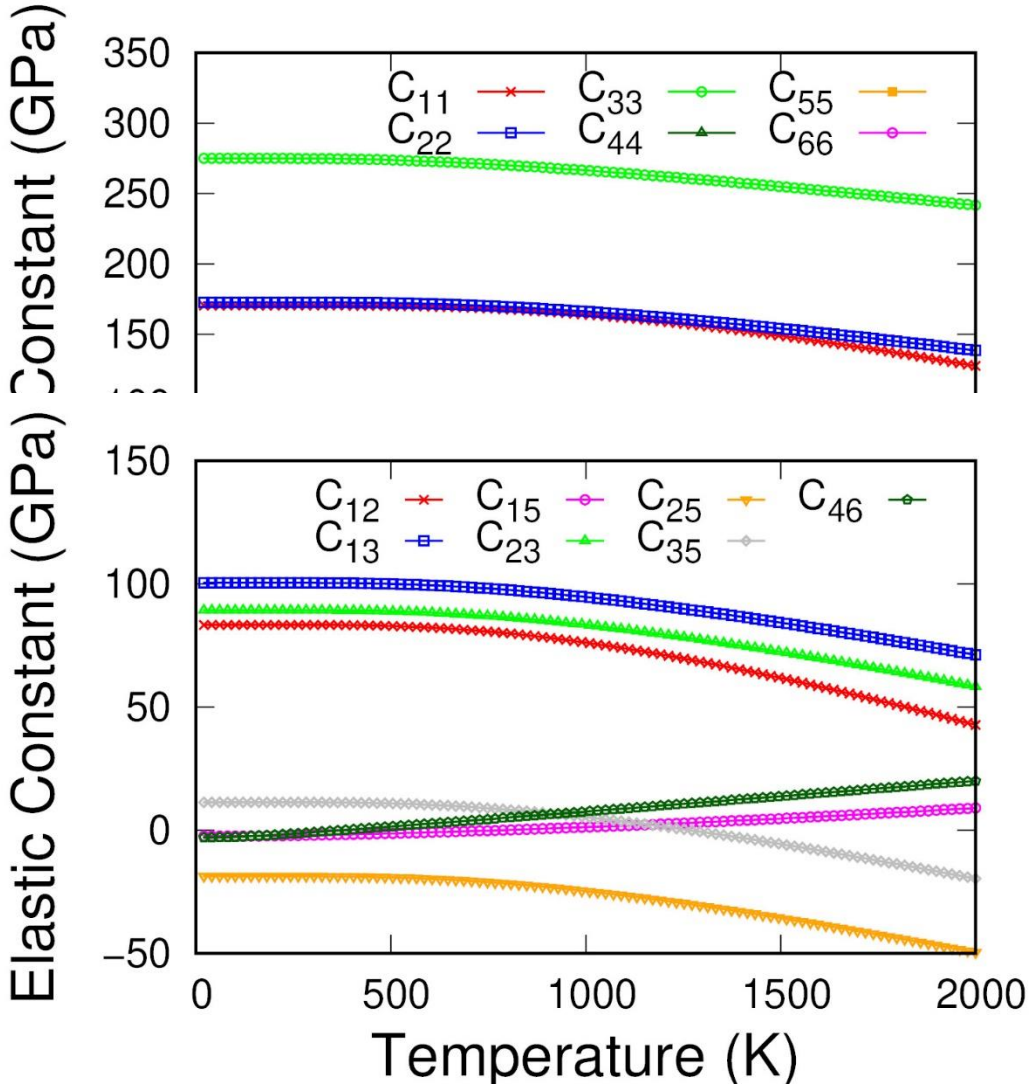

S. Hao, R. Oleksak, O. Dorgan, M. Gao, Acta Materialia, 258 (2023), 119225

Elastic Anisotropy

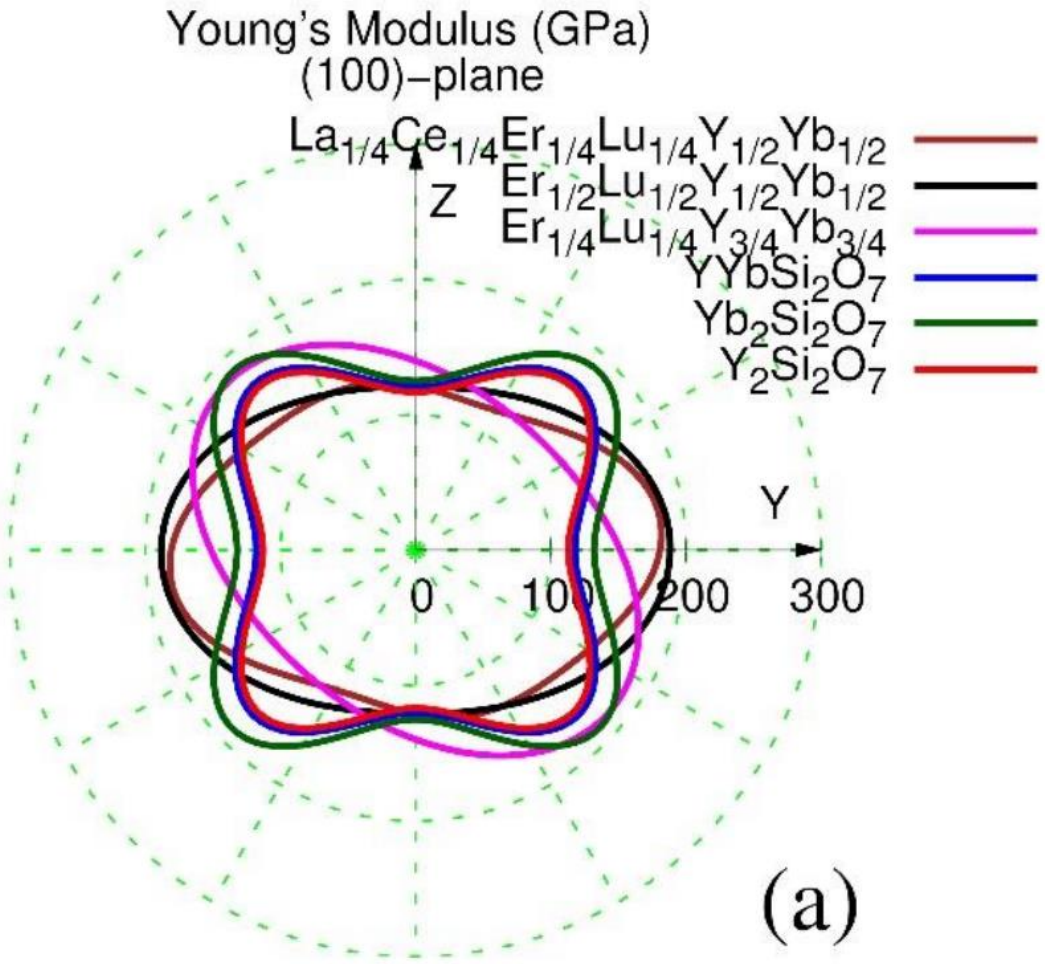

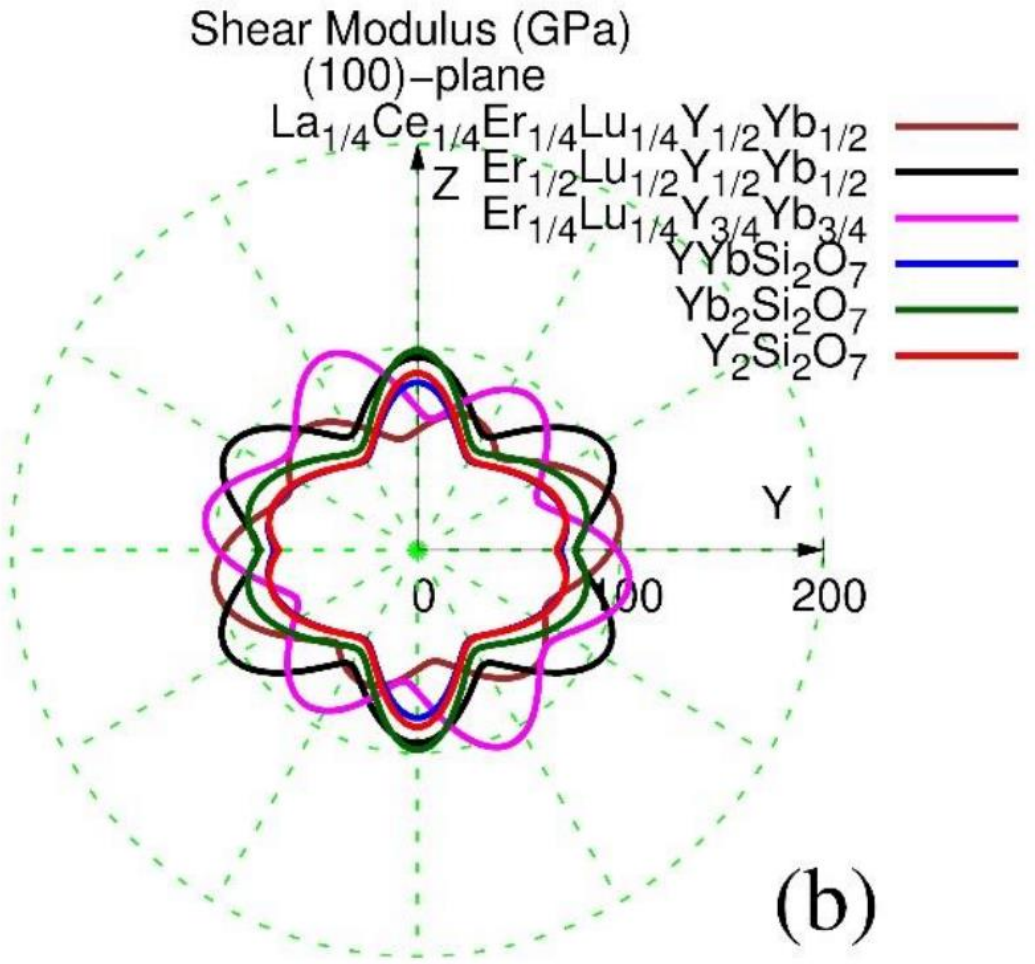

Elastic anisotropy plays a crucial role in understanding the formation of microcracks within coatings. A low modulus corresponds to a direction with low fracture energy.

S. Hao, R. Oleksak, O. Dorgan, M. Gao, Acta Materialia, 258 (2023), 119225

Temperature Dependent Moduli

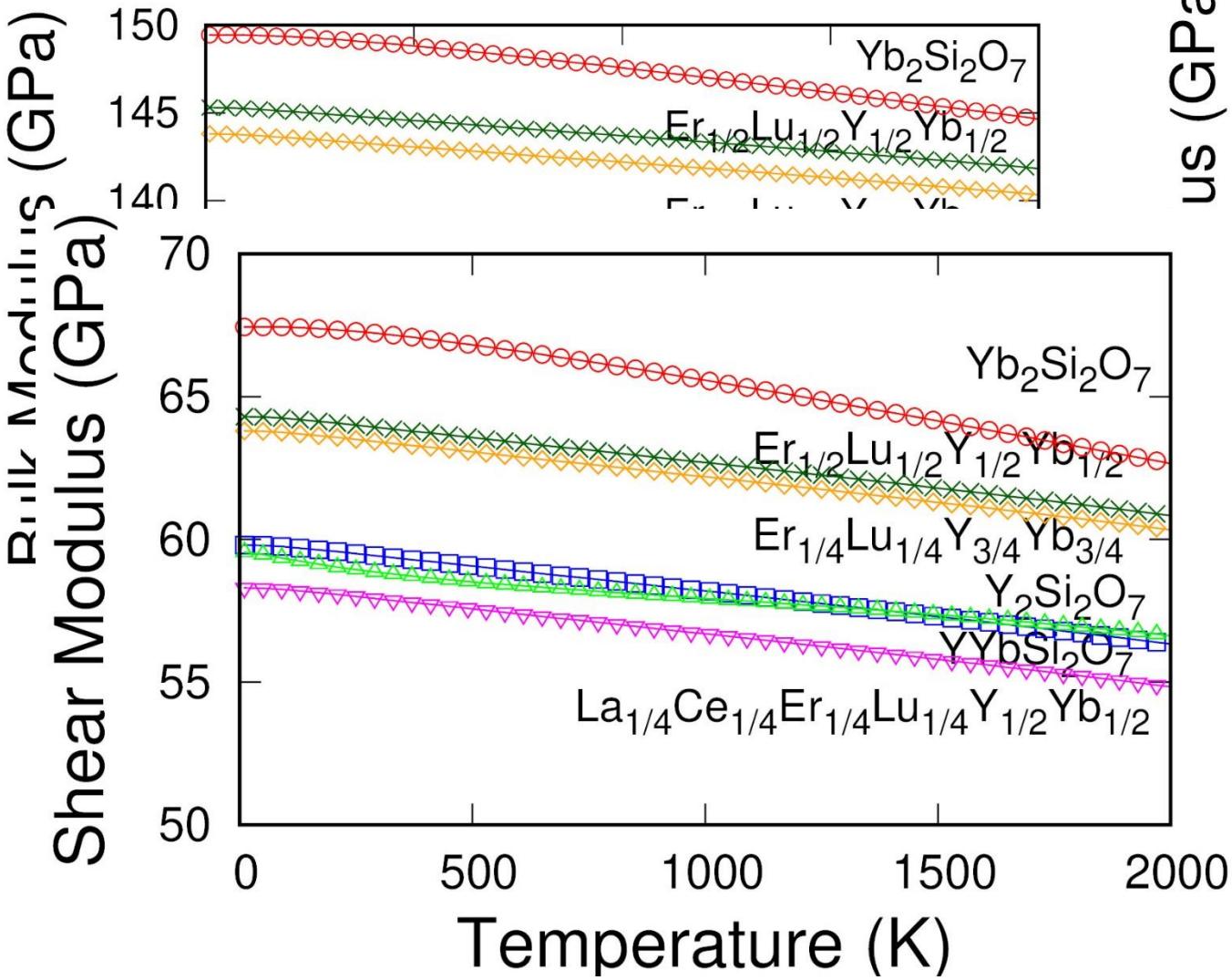

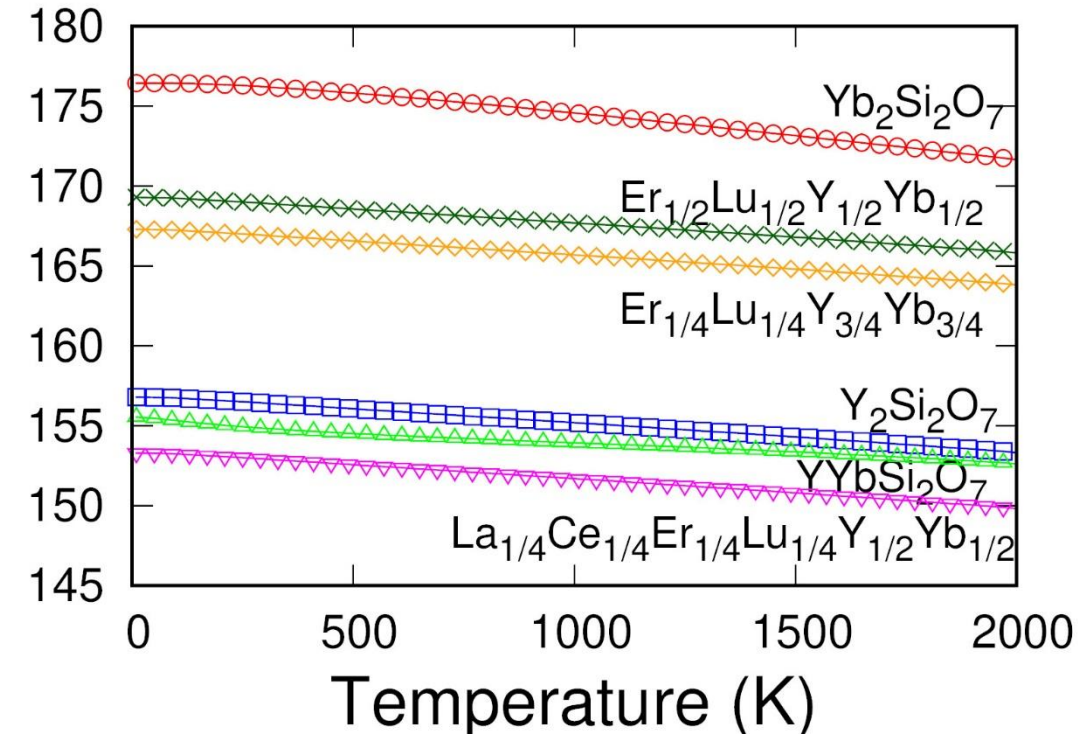

Moduli exhibit decreasing behavior as temperature.

S. Hao, R. Oleksak, O. Dorgan, M. Gao, Acta Materialia, 258 (2023), 119225

Correlation Analysis

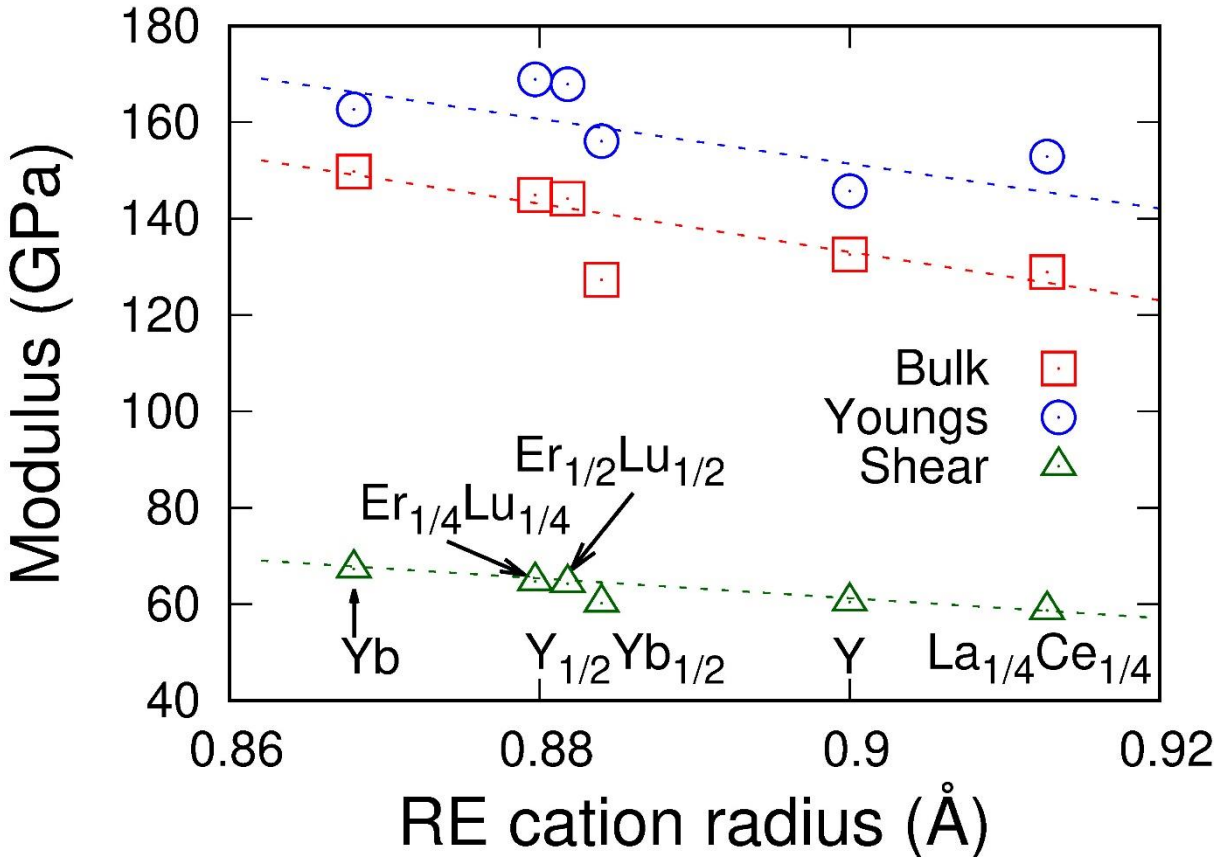

$$r = \frac{\Sigma_{i=1}^{n}(X_i-\bar{X})(Y_i-\bar{Y})}{\sqrt{\sum_{i=1}^{n}(X_i-\bar{X})^2}\sqrt{\sum_{i=1}^{n}(Y_i-\bar{Y})^2}}$$

$$RMSD = \sqrt{\frac{\sum_{i=1}^{n}(Y_i-\bar{Y})^2}{(N-1)\sum_{i=1}^{n}(\bar{Y})^2}}$$

The closer the magnitudes to 1 (or -1), the stronger the correlation, while values closer to zero suggest a weaker correlation. A negative correlation indicates that when one variable increases, the other variable decreases.

Relative strong negative Pearson correlations: -0.76,-0.71, -0.89 of bulk, Young's and shear moduli with radius of RE.
CTE 0.68. LTC -0.21.

S. Hao, R. Oleksak, O. Dorgan, M. Gao, Acta Materialia, 258 (2023), 119225

Summary on β Phase

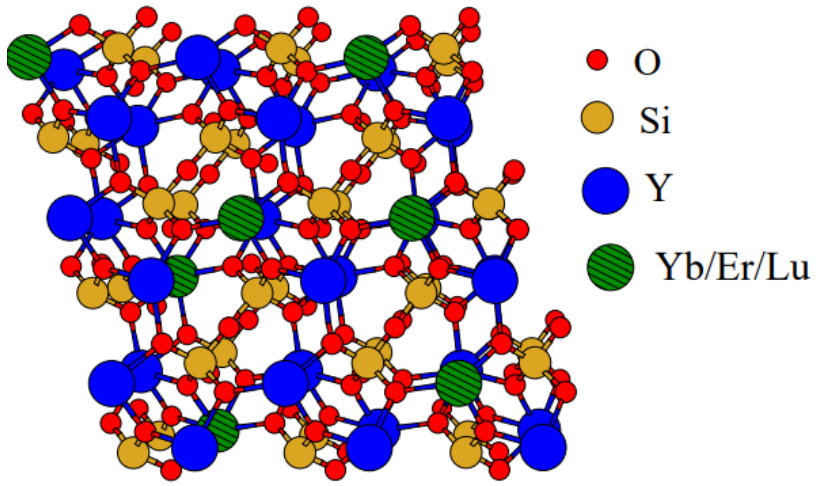

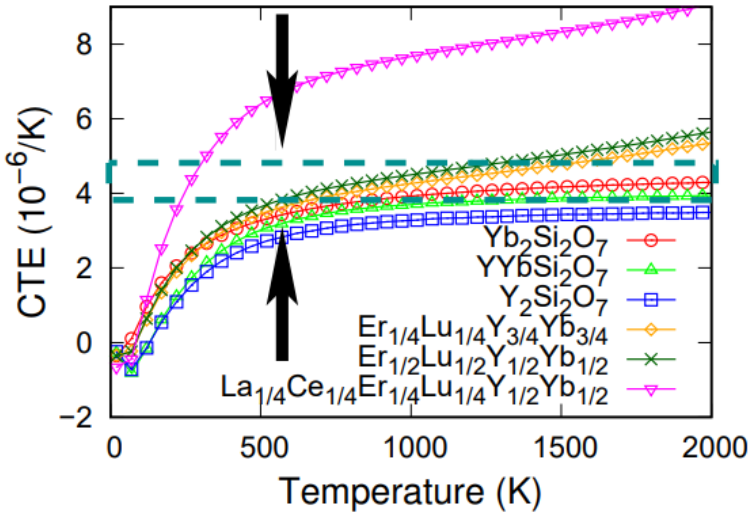

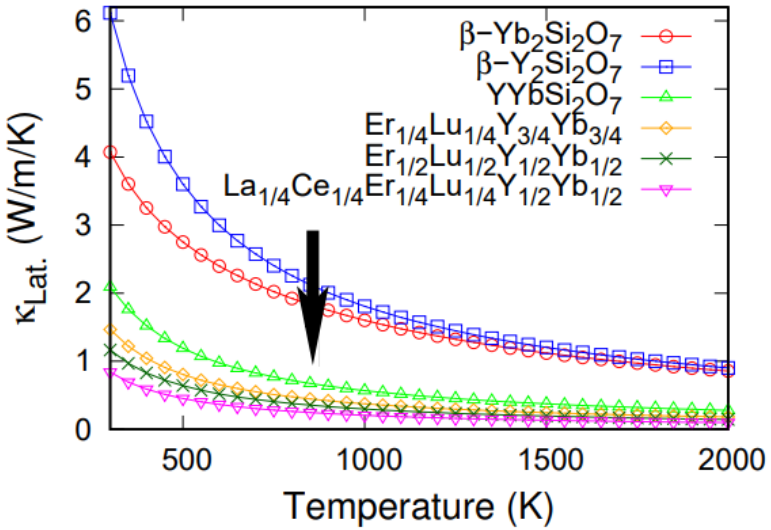

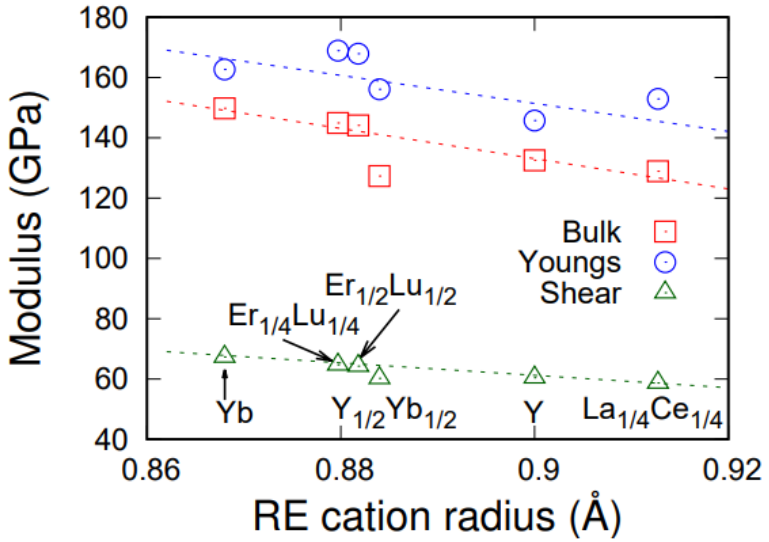

- Using combinatory chemistry and first-principles based methodologies.
- We predict the mechanical properties of solid solutions of $(ErLuYYb)_2Si_2O_7$ are not deteriorated.
- CTE of $Er_{1/4}Lu_{1/4}Y_{3/4}Yb_{3/4}Si_2O_7$ and $Er_{1/2}Lu_{1/2}Y_{1/2}Yb_{1/2}Si_2O_7$ exhibits good match with SiC with much decreased lattice thermal conductivity.

S. Hao, R. Oleksak, O. Dorgan, M. Gao, Acta Materialia, 258 (2023), 119225

$La_2Si_2O_7$ and $Ce_2Si_2O_7$

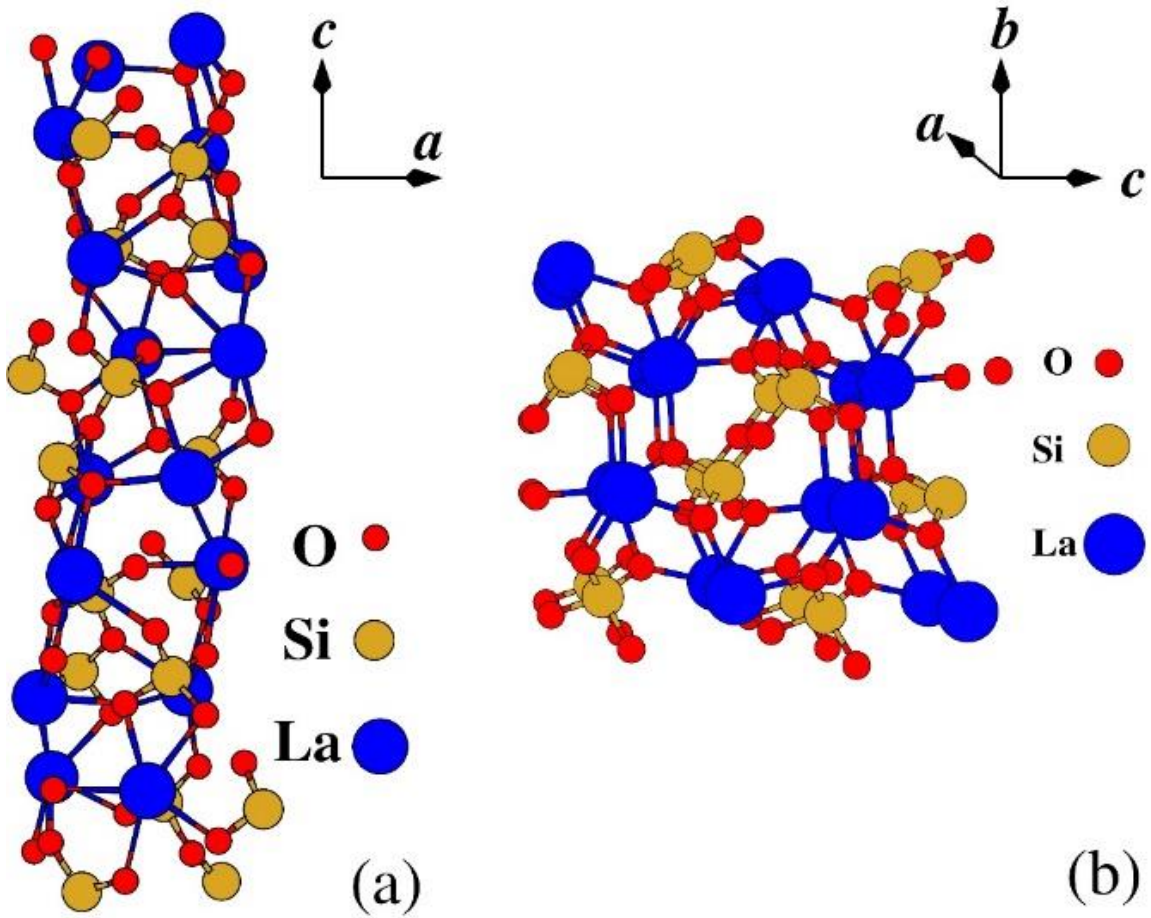

(a)The atomic structure of low temperature A-phase of $La_2Si_2O_7$ with the space group of $P4_1$. (b) The atomic structure of high temperature G-phase $La_2Si_2O_7$ with space group of $P2_1/C$. The corresponding A- and G-phase of $Ce_2Si_2O_7$ are the same by simply replacing La with Ce.

$La_2Si_2O_7$ and $Ce_2Si_2O_7$

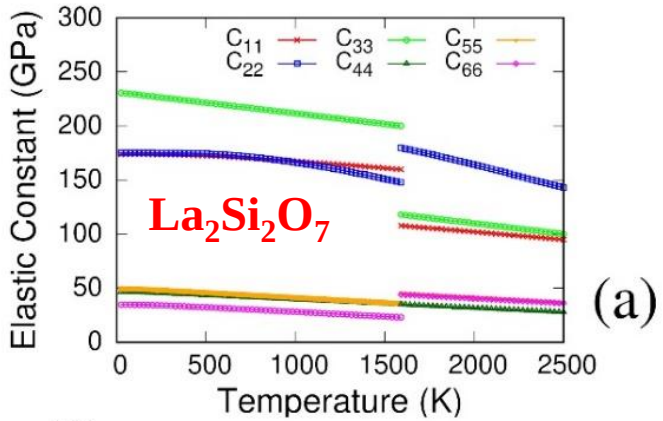

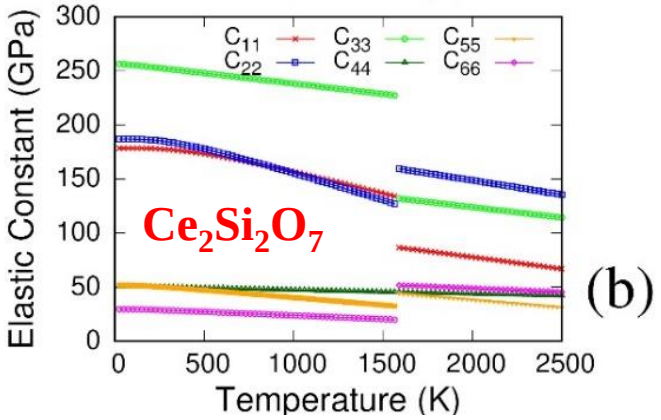

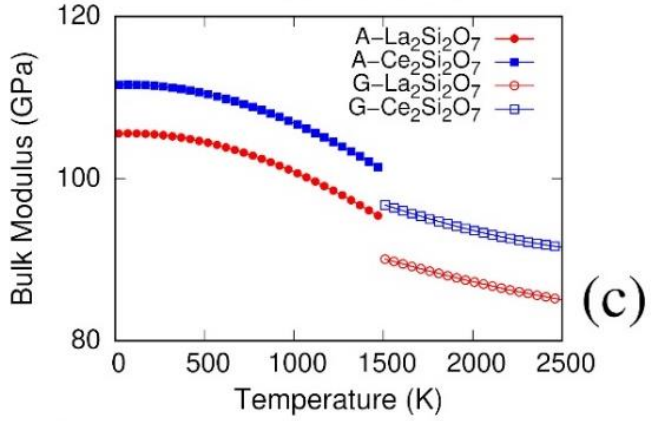

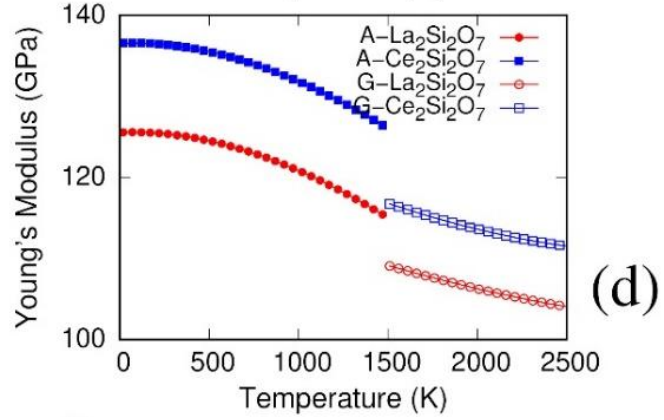

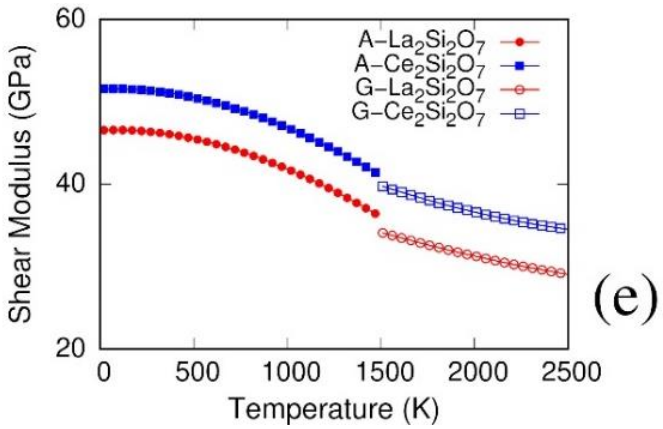

The temperature-dependent elastic constants for (a) $La_2Si_2O_7$ and (b) $Ce_2Si_2O_7$, and the temperature-dependent (c) bulk modulus, (d) Young's modulus and shear modulus.

$La_2Si_2O_7$ and $Ce_2Si_2O_7$

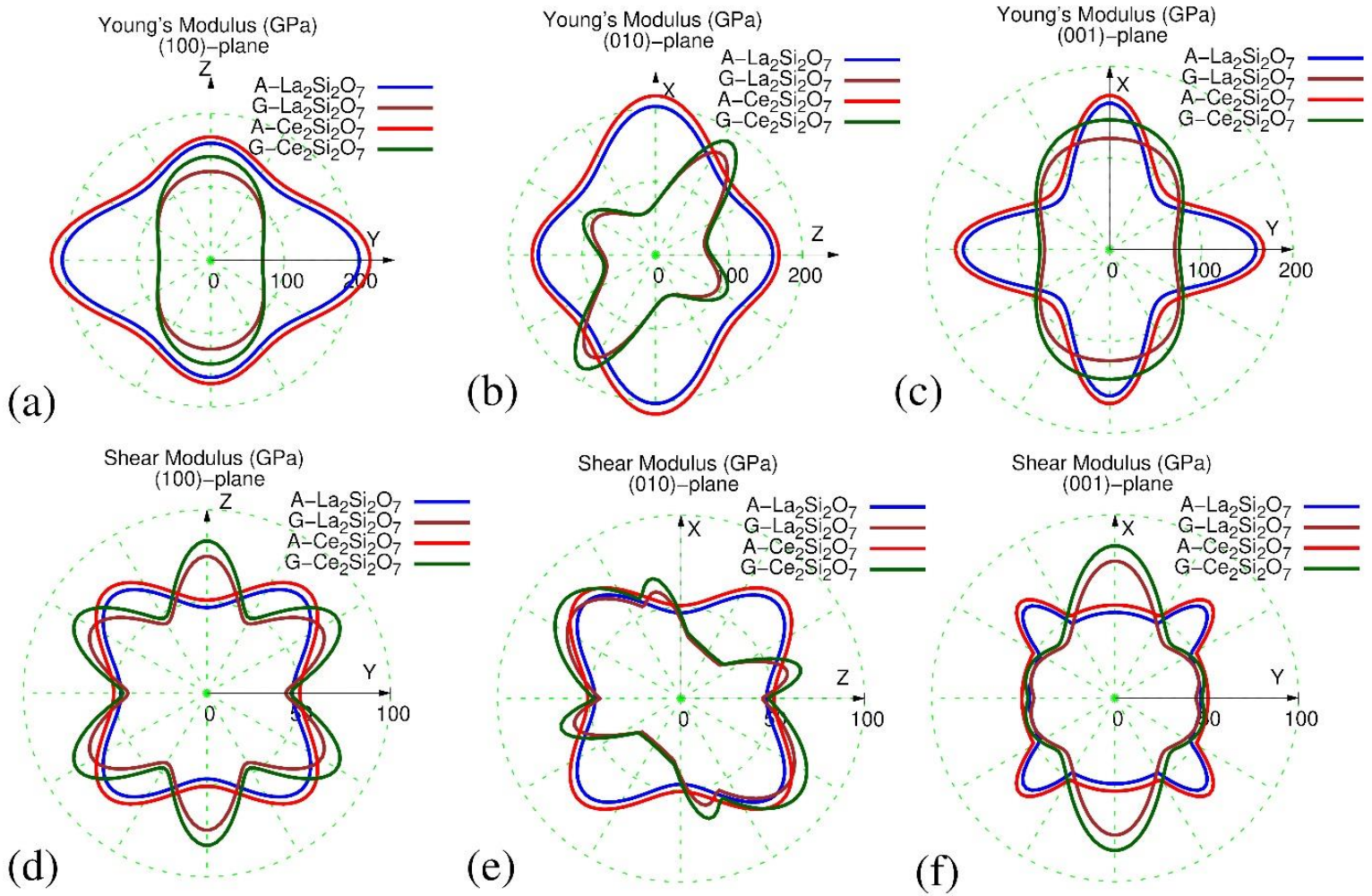

Elastic anisotropy of Young's modulus and shear modulus in different plane of (a,d) (100), (b,e) (010), and (c,f) (001), for all four phases of $La_2Si_2O_7$ and $Ce_2Si_2O_7$, respectively.

$La_2Si_2O_7$ and $Ce_2Si_2O_7$

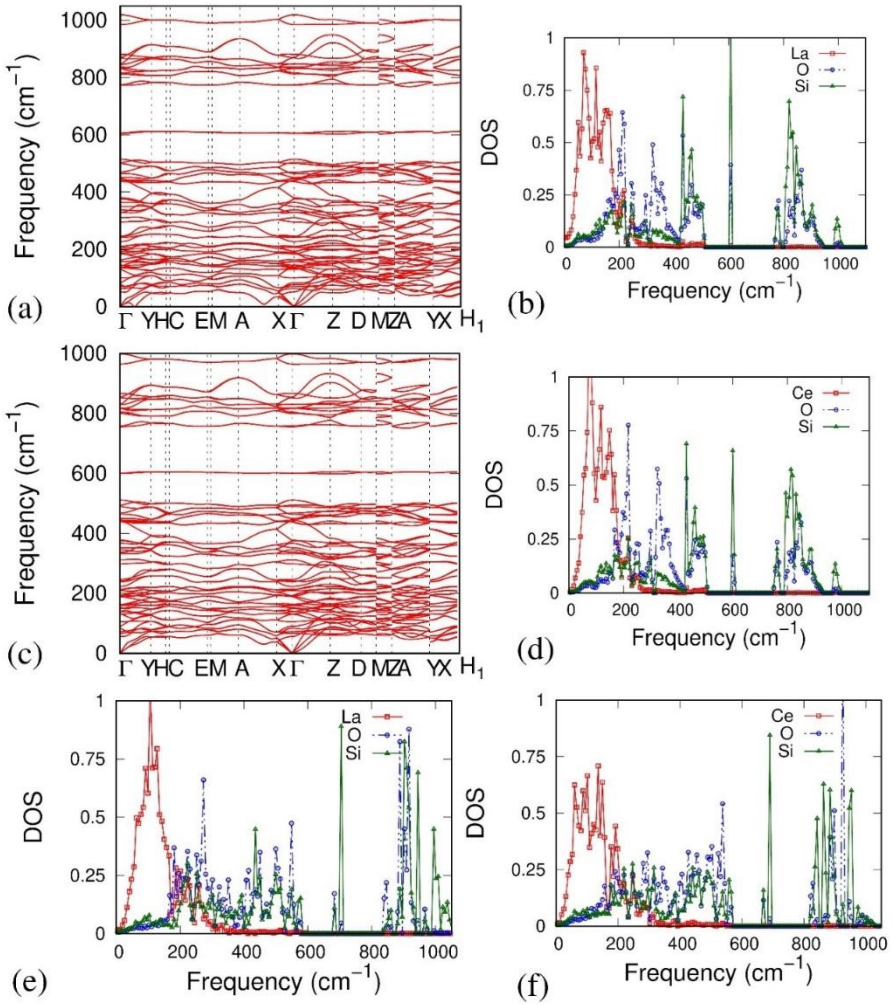

The phonon dispersion (a, c) and projected phonon density of states (b, d) at corresponding equilibrium volume V_0 for the G-phase $La_2Si_2O_7$ (a, b) and G-phase $Ce_2Si_2O_7$ (c, d). The vibrational projected phonon density of states of A-phase $La_2Si_2O_7$ (e) and A-phase $Ce_2Si_2O_7$ (f).

$La_2Si_2O_7$ and $Ce_2Si_2O_7$

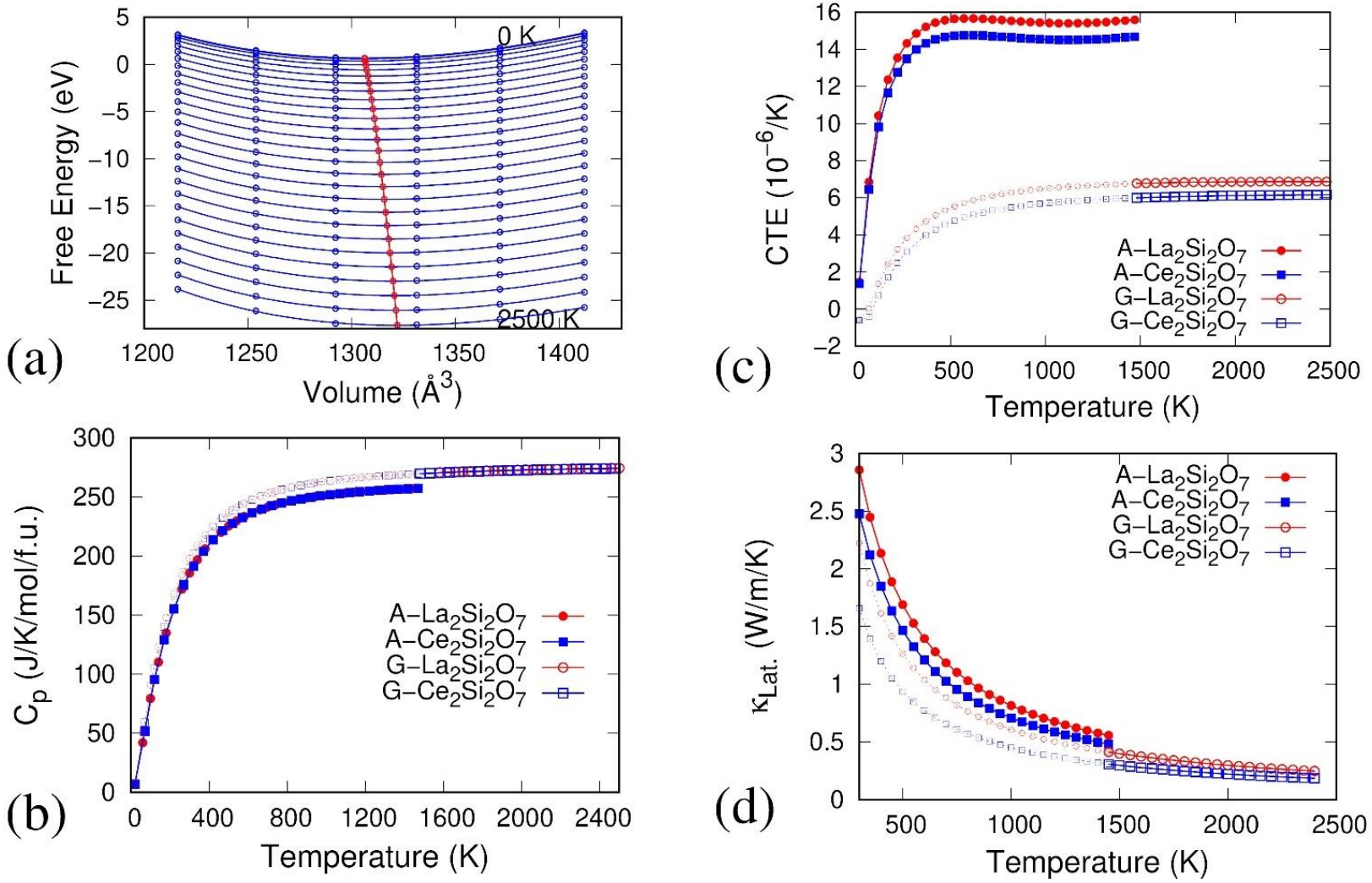

(a) An example of free energy as a function of volume and temperature for G-$La_2Si_2O_7$ system. The blue dots and blue lines are respectively DFT calculated values and fitted results. The red dots represent the minimum free energy at corresponding volume and temperatures ranging from 0 to 2500 K with a step of 100 K. (b) Heat capacity (c) coefficients of thermal expansion and (d) lattice thermal conductivity of A- and G-phases of $La_2Si_2O_7$ and $Ce_2Si_2O_7$. The low temperature A-phase data are plotted in a range of (0-1470 K), the high temperature G phase data are depicted in a range of (1470-2500 K).

S. Hao, R.P. Oleksak, Ö.N. Doğan, M.C. Gao, Low-cost thermal/environmental barrier coatings: A first-principles study, Computational Materials Science 230 (2023) 112541.

Summary on A-Phase and G-Phase

- Employed density functional theory-based techniques to predict the thermodynamic, mechanical, and thermal properties of the A- and G-phase of abundant rare earth disilicates, specifically La2Si2O7 and Ce2Si2O7, with the aim of assessing their suitability as low-cost materials as T/EBC.
- Utilized the strain-energy method to derive elastic constants by computing the second derivatives of the total energy with respect to the corresponding lattice strains.
- Verified the mechanical stability of these structures as the calculated elastic constants satisfying established stability criteria. The average polycrystalline elastic properties were estimated using the Voigt-Reuss-Hill's schemes.
- Using phonon calculations at varying volumes under the quasi-harmonic approximation, we computed the system's Helmholtz free energy as a function of both volume and temperature. This enabled us to obtain the values for heat capacity and CTE. Finally, we evaluated the lattice thermal conductivities by using Debye-Callaway model considering three phonon processes.
- The transition from A-phase to G-phase causes notable alterations in crystal symmetry and lattice parameters, and accordingly, CTE and lattice thermal conductivities. These transformations could potentially impose limitations on their suitability for use as T/EBC materials.
- Among all calculated results, the G-phase of Ce2Si2O7 displays characteristics that make it a potentially strong candidate for protecting SiC-based ceramic matrix composites at high temperatures. Specifically, it has an extremely low lattice thermal conductivity of approximately 0.26 W/m/K at 1500 K and a low CTE (average ≈6.9×10-6 K-1) that matches well with SiC.
- However, the substantial difference in CTE values between the A-phase and G-phase of Ce2Si2O7 poses obvious challenges during thermal cycling. Methods to stabilize the high-temperature G-phase at lower temperatures, and/or to slow down the kinetics of transformation, may enable the use of these inexpensive and abundant materials as effective T/EBC for protecting SiC-based composites and other high temperature materials.

S. Hao, R.P. Oleksak, Ö.N. Doğan, M.C. Gao, Low-cost thermal/environmental barrier coatings: A first-principles study, Computational Materials Science 230 (2023) 112541.

Acknowledgments

This work was performed in support of the U.S. Department of Energy's (DOE) Fossil Energy Crosscutting Technology Research Program. The research was executed through the National Energy Technology Laboratory's (NETL) Research and Innovation Centers Advanced Materials Development Field Work Proposal. This research used resources of the National Energy Research Scientific Computing Center (NERSC), a DOE Office of Science User Facility supported by the Office of Science.

Disclaimer

This project was funded by the United States Department of Energy, National Energy Technology Laboratory, in part, through a site support contract. Neither the United States Government nor any agency thereof, nor any of their employees, nor the support contractor, nor any of their employees, makes any warranty, express or implied, or assumes any legal liability or responsibility for the accuracy, completeness, or usefulness of any information, apparatus, product, or process disclosed, or represents that its use would not infringe privately owned rights. Reference herein to any specific commercial product, process, or service by trade name, trademark, manufacturer, or otherwise does not necessarily constitute or imply its endorsement, recommendation, or favoring by the United States Government or any agency thereof. The views and opinions of authors expressed herein do not necessarily state or reflect those of the United States Government or any agency thereof.

NETL RESOURCES

VISIT US AT: **www.NETL.DOE.gov**

@NETL_DOE

@NETL_DOE

@NationalEnergyTechnologyLaboratory

CONTACT: